Article

*Discovery Medicine* 2023; 35(179): 995–1014
https://doi.org/10.24976/Discov.Med.202335179.96

# LncRNA *SLC1A5-AS/MZF1/ASCT2* Axis Contributes to Malignant Progression of Hepatocellular Carcinoma

Jiawen Jiang[1,†], Wei Dong[2,†], Wen Zhang[1], Qian Wang[3], Ruyi Wang[4], Jiaxu Wang[1], Hao Wu[1], Hui Dong[2], Robert Chunhua Zhao[1,5], Jiao Wang[1,*], Zhe Li[1,*]

[1]School of Life Sciences, Shanghai University, 200444 Shanghai, China
[2]Department of Pathology, Eastern Hepatobiliary Surgery Hospital, the Second Military Medical University, 200438 Shanghai, China
[3]Shanghai Public Health Clinical Center, Fudan University, 201500 Shanghai, China
[4]University of Wisconsin–Madison, Brogden Psychology Bldg, Madison, WI 53706, USA
[5]Institute of Basic Medical Sciences Chinese Academy of Medical Sciences, School of Basic Medicine Peking Union Medical College, 100730 Beijing, China
*Correspondence: jo717@shu.edu.cn (Jiao Wang); zhe_li0913@shu.edu.cn; lzshanghai@163.com (Zhe Li)
†These authors contributed equally.
Published: 1 December 2023

**Background: Hypoxia is a pivotal factor influencing cellular gene expression and contributing to the malignant progression of tumors. Metabolic anomalies under hypoxic conditions are predominantly mediated by mitochondria. Nonetheless, the exploration of hypoxia-induced long noncoding RNAs (lncRNAs) associated with mitochondria remains largely uncharted.**
**Methods: We established hypoxia cell models using primary human hepatocytes (PHH) and hepatocellular carcinoma (HCC) cell lines. We isolated mitochondria for high-throughput sequencing to investigate the roles of candidate lncRNAs in HCC progression. We employed *in vitro* and *in vivo* assays to evaluate the functions of solute carrier family 1 member 5 antisense lncRNA (*SLC1A5-AS*). RNA-seq was utilized to scrutinize the comprehensive genome profile regulated by *SLC1A5-AS* in HCC. Subsequently, quantitative real-time polymerase chain reaction (qRT-PCR) and western blot analysis were utilized to validate the expression of alanine-serine-cysteine transporter 2 (*ASCT2*, encoded by the *SLC1A5* gene), and a glutamine uptake assay was employed to estimate the glutamine uptake capacity of Huh-7 cells after *SLC1A5-AS* overexpression. To delve into the mechanisms governing the regulation of SLC1A5 expression by *SLC1A5-AS*, we employed a biotin-labeled *SLC1A5-AS* probe in conjunction with a western blot assay to confirm the interactions between *SLC1A5-AS* and candidate transcription factors. Luciferase reporter assays and chromatin immunoprecipitation (ChIP) were utilized to authenticate the effects of the predicted transcription factors on *SLC1A5* promoter activity.**
**Results: Following the screening, we identified *CTB-147N14.6*, derived from the antisense strand of the *SLC1A5* gene, which we have named *SLC1A5-AS*. *SLC1A5-AS* exhibited significantly elevated expression levels in HCC tissue and was associated with poor prognosis in HCC patients. *In vitro* and *in vivo* assays revealed that the overexpression of *SLC1A5-AS* significantly heightened cell invasion and metastasis. RNA-seq data unveiled *SLC1A5-AS* involvement in glutamine metabolism, left-handed amino (L-amino) acid transmembrane transporter activity, and the nuclear factor kappa-B (NF-$\kappa$B) signaling pathway. Overexpression of *SLC1A5-AS* markedly increased *ASCT2* mRNA/protein levels, thereby enhancing glutamine uptake and promoting the growth and metastasis of HCC cells. Mechanistically, higher RNA levels of *SLC1A5-AS* directly bound with myeloid zinc finger 1 (*MZF1*), acting as a transcriptional repressor, thus diminishing its binding to the *SLC1A5* promoter region.**
**Conclusions: Our findings unveil a novel role for the lncRNA *SLC1A5-AS* in glutamine metabolism, suggesting that targeting *SLC1A5-AS*/*MZF1*, in conjunction with *ASCT2* inhibitor treatment, could be a potential therapeutic strategy for this disease.**

**Keywords:** hepatocellular carcinoma; hypoxia; lncRNA *SLC1A5-AS*/*MZF1*/*ASCT2*; glutamine metabolism

## Introduction

Hepatocellular carcinoma (HCC) constitutes approximately 90% of primary liver cancers and is associated with an exceptionally high mortality rate among human malignancies [1]. The primary treatments for HCC, following the Barcelona Clinic Liver Cancer (BCLC) strategy, encompass surgical interventions, ablation procedures, and transarterial chemoembolization (TACE) for early-stage cases (BCLC 0-B), while chemotherapy is the principal approach for late-stage HCC (BCLC C-D). Nevertheless, chemotherapy medications often bring about adverse side effects, and resistance can develop [2]. There is an urgent need to explore innovative and effective strategies for treating HCC. The growth and expansion of tumor cells often lead to the development of a hypoxic microenvironment

[3,4], with mitochondrial reprogramming being primarily responsible [5]. Mitochondrial function is intricately linked to the development of cancer [6,7]. In response to hypoxic stress, nutrient scarcity, and metabolic disruptions, mitochondria adapt by integrating multiple metabolic pathways, including the tricarboxylic acid (TCA) cycle, fatty acid oxidation (FAO), amino acid oxidation (AAO), and oxidative phosphorylation (OXPHOS), to support the growth and survival of tumor cells [8]. Therefore, gaining a deep understanding of mitochondrial function abnormalities is crucial for investigating the molecular mechanisms behind HCC development and progression.

Recent genome-wide transcriptome studies have revealed that approximately 80% of human genes are transcribed as noncoding RNAs (ncRNAs) [9]. Long noncoding RNAs (lncRNAs) are transcripts exceeding 200 nucleotides in length and do not encode proteins. They have been shown to play vital regulatory roles, including the regulation of gene expression, RNA processing, and translation, thereby significantly impacting various cellular functions and the regulation of physiological processes, as well as the development of diseases [10–14]. Although it has been reported that long noncoding RNAs regulate mitochondrial function [15] and tumor metabolism [16], there remains a need for further exploration of mitochondria-associated lncRNAs under hypoxic conditions in HCC, to identify new molecular targets for therapeutic intervention.

In this study, we have identified an antisense lncRNA related to mitochondria, previously known as *CTB-147N14.6*, which we have renamed as solute carrier family 1 member 5 antisense lncRNA (*SLC1A5-AS*). This lncRNA exhibits elevated levels of RNA under hypoxic conditions and functions as an oncogene in HCC. It achieves this by increasing both the mRNA and protein levels of SLC1A5, primarily by inhibiting myeloid zinc finger 1 (*MZF1*) from binding to the promoter region of *SLC1A5*. The overexpression of *SLC1A5*, in turn, enhances the uptake of glutamine by the cells. Our data strongly suggest that *SLC1A5-AS* is an oncogenic lncRNA and represents a promising therapeutic target when combined with glutamine inhibitors for the treatment of HCC.

## Materials and Methods

### *Patients and Ethical Statement*

Sixty-seven pairs of HCC tissues and their corresponding adjacent normal liver tissues were retrieved from the surgical specimen archives of the Eastern Hepatobiliary Surgery Hospital, which is affiliated with the Naval Medical University. These tissue specimens were meticulously preserved at –80 °C to facilitate RNA extraction. The utilization of human clinical specimens in this study received approval from the review board of Second Military Medical University, and every patient provided written informed consent for the use of their resected tissues for research purposes. A pathologist meticulously graded and analyzed the clinicopathological characteristics of HCC patients, encompassing aspects such as tumor microsatellite formation, tumor encapsulation, venous invasion, cellular differentiation, direct liver invasion, hepatitis B surface antigen presence, tumor size, and pathological tumor-node-metastasis (pTNM) tumor stage. All clinical investigations were scrupulously conducted in full accordance with the principles outlined in the Declaration of Helsinki. The results of the multivariate Cox regression analyses of *SLC1A5-AS* in liver cancer concerning clinicopathologic factors can be found in **Supplementary Table 1**.

### *Cell Lines and Reagents*

The human liver cancer cell lines Hep-3B (cat. no. HB-8064) and Hep G2 (cat. no. HB-8065) were obtained from the American Type Culture Collection (ATCC Manassas, VA, USA). Additionally, HEK293T cells (cat. no. CRL3216) were sourced from the same institution. Huh-7 cells (cat. no. 3101HUMSCSP526) were purchased from the Shanghai Cell Bank Type Culture Collection Committee (CBTCCC, Shanghai, China). These cell lines were individually cultured and maintained in dulbecco's modified eagle medium (DMEM) (cat. no. 11995040, Thermo Fisher, MA, USA), which was supplemented with 10% fetal bovine serum (FBS) (cat. no. 10091148, Thermo Fisher, MA, USA), and penicillin (100 U/mL)/streptomycin (100 µg/mL) (cat. no. 15140, Thermo Fisher, MA, USA). Culturing was performed at 37 °C in an atmosphere containing 5% $CO_2$ (vol/vol). Hep-3B and Hep G2 cell lines were similarly cultured and maintained in eagle's minimal essential medium (EMEM) (cat. no. 30-2003, ATCC, Manassas, VA, USA), supplemented with 10% FBS and penicillin (100 U/mL)/streptomycin (100 µg/mL). These cultures were also maintained at 37 °C with 5% $CO_2$. To ensure the quality of these cell lines, authentication was performed using short tandem repeats (STR) profiling, and they were confirmed to be free from mycoplasma contamination. Routine examinations, including assessments of cell morphology and mycoplasma presence, were carried out. Phosphate-buffered saline (PBS) (cat. no. 162496) and dimethyl sulfoxide (DMSO) (cat. no. 196055) were purchased from MP Biomedicals (Santa Ana, CA, USA).

### *Thawing, Seeding, and Monolayer Culture of Primary Human Hepatocytes*

Plateable cryopreserved human hepatocytes (from 10 male donors) were procured from Lonza (cat. no. HUCS10PM, Basel, Switzerland). To recover these hepatocytes, the Hepatocyte Thaw Medium (cat. no. CM7500, Gibco, CA, USA) was employed as per the provided instructions. In brief, the Hepatocyte Thaw Medium was pre-warmed to 37 °C. The cryopreserved hepatocytes were thawed in a 37 °C water bath for less than 2 minutes. Subsequently, the hepatocytes were transferred to the hep-

atocyte thaw medium and centrifuged at room temperature (100 g, 10 minutes), with the removal of the supernatant. Following this, 3 mL of plating medium prewarmed to 37 °C was added to the hepatocytes and gently shaken to re-suspend the cells. These hepatocytes were then seeded on a culture plate coated with collagen type I (cat. no. A1048301, Thermo Fisher, MA, USA) and incubated in a Null culture medium at 37 °C with 5% $CO_2$ for 6 hours. Six hours after seeding, adherent primary human hepatocytes (PHH) were cultured in a serum-free 5C medium. After 24 hours of cultivation, the hepatocytes were maintained in a commercial hepatocyte culture medium (HCM) (cat. no. CC-3198, Lonza, Basel, Switzerland), with daily renewal. The Null culture medium typically used for hepatocytes consisted of Williams' medium E (cat. no. 22551089, Gibco, CA, USA), supplemented with B27 (cat. no. A3582801), Glutamax (cat. no. 35050061), and Pen/Strep. The plating medium comprised HCM supplemented with 10% FBS. The 5C medium was prepared by supplementing the Null culture medium with 20 µM forskolin (cat. no. 6652995, Peprotech, NJ, USA), 10 µM SB431542 (cat. no. 3014193), 0.5 µM IWP2 (cat. no. 6866167), 5 µM DAPT (cat. no. AG-CR1-0016, Adipogen, CA, USA), and 0.1 µM LDN193189 (cat. no. 1066208, Peprotech, NJ, USA). The cells were authenticated through STR profiling and confirmed to be free of mycoplasma contamination.

### *Construct Hypoxia Cell Models with Cobalt Chloride ($CoCl_2$)*

$CoCl_2$ (0.1 M/mL), sourced from Sigma-Aldrich (cat. no. 7646-79-9, St. Louis, MO, USA), was used for the experiments. Before the $CoCl_2$ treatment (at a final concentration of 200 µM), PHH, Huh-7, and Hep-3B were cultured without serum and antibiotics for 12 hours, which served as a starvation treatment [17]. Each group was treated with $CoCl_2$ individually for 6 and 12 hours to establish the hypoxia models. Subsequently, we assessed the expression of several key genes, including solute carrier family 2 member 1 (*GLUT1*), carbonic anhydrase 9 (*CA9*), pyruvate dehydrogenase kinase 1 (*PDK1*), and hypoxia-inducible factor-1 alpha (*HIF-1α*), at the RNA level in these cell lines to confirm the successful construction of the hypoxia model [4,18].

### *Isolation of Mitochondria*

All procedures were conducted in accordance with the guidelines provided in the Mitochondria Isolation Kit for Cultured Cells (cat. no. 89874), which was acquired from Thermo Fisher in MA, USA. The cell suspension was initially collected by centrifugation at 850 ×g for 2 minutes in a 2.0 mL microcentrifuge tube, and the supernatant was carefully decanted. Subsequently, 800 microliters of reagent A were introduced. The mixture was vortexed for 5 seconds at medium speed, and the tubes were then placed on ice for a 2-minute incubation period. Following this, 10 µL of reagent B was added, and a 5-second vortexing at maximum speed was carried out. The tubes were incubated on ice for 5 minutes, with vigorous vortexing at maximum speed performed every minute. Next, 800 microliters of reagent C were added, and the contents were mixed by gently turning the tube upside down several times. The cytoplasmic and nuclear components were then separated through differential centrifugation, after which 500 µL of reagent C was added, and the mixture was centrifuged at 12,000 ×g for 5 minutes. The supernatant was discarded to isolate the mitochondrial precipitate.

### *Isolation of Total RNAs from the Patients' Liver Tissues, Cell Lines, and Mitochondria*

In this study, total RNA was isolated using TRIzol reagent (cat. no. R1100, Solarbio Life Sciences, Beijing, China) following the manufacturer's protocol. Briefly, 1 mL TRIzol Reagent was added, and the sample was suspended thoroughly. Next, 0.2 times the volume of trichloromethane (cat. no. 67-66-3, Sinopharm Chemical Reagent Co., Ltd., Shanghai, China) was added to a tube containing the lysate. The tube was shaken completely for 30 seconds on a shaker and left for 2–3 minutes at room temperature. Then, the samples were centrifuged at 12,000 ×g for 10 minutes at 4 °C, and the upper aqueous phase containing the total RNA was transferred into a new tube. Next, 0.5 mL of isopropanol (cat. no. 67-63-0, Sinopharm Chemical Reagent Co., Ltd., Shanghai, China) was added and mixed by inversion, precipitated for 10 minutes at room temperature, and then centrifuged at 12,000 ×g for 10 minutes at 4 °C. The supernatant was discarded, and 1 mL of 75% ethanol was added to clean the RNA precipitate, followed by centrifugation at 12,000 ×g for 2 minutes at 4 °C. Next, the supernatant was discarded and dried at room temperature for 5–10 minutes. Finally, the appropriate amount of diethylpyrocarbonate (DEPC)-treated water was added to dissolve the RNA.

### *First-Strand cDNA Synthesis and Quantitative Real-Time PCR*

First-strand cDNA synthesis from total RNA was conducted using the PrimeScript™ RT Master Mix (cat. no. RR036A, Takara, Dalian, China). In this process, 1 µg of total RNA was utilized in the RT system. To measure relative RNA levels via real-time quantitative PCR (qPCR), a CFX96TM Real-Time System was employed, and the TB Green® Premix Ex Taq™ II method (cat. no. RR820B, Takara, Dalian, China), was used. The reaction system comprised TB Green Premix Ex Taq II (10 µL), specific primers (2 µL), cDNA template (4 µL), and ultrapure water to a total volume of 20 µL. The gene-specific primer sequences can be found in **Supplementary Table 2**. *β-actin*, *U2*, and *GAPDH* were employed as internal controls for quantifying the mRNA levels of the mentioned genes. *β-actin* and *GAPDH* were used as internal references for the

entire cellular components or the cytoplasmic component. *U2* (Sangon Biotech, Shanghai) served as an internal reference for the nuclear component. Furthermore, the comparative CT ($2^{-\Delta\Delta CT}$) method was employed to determine the relative RNA levels.

### *Subcellular Localization*

The isolation of nuclear and cytoplasmic components from HCC cells involved the following sequential steps: First, $1 \times 10^6$ cells were gathered in 1.5 mL Eppendorf (EP) tubes, and after centrifugation at 3000 rpm for 3 minutes, the supernatant was carefully discarded. Second, 300 µL of cytoplasmic lysis buffer, consisting of 20 mM Tris-HCl, 10 mM NaCl, 0.2% NP-40, 2 mM $MgCl_2$, and brought up to a final volume of 50 mL with ultrapure water, was added to the cells. The mixture was gently vortexed and left on ice for 10 minutes to facilitate cell lysis. Subsequently, the tubes were subjected to centrifugation at 12,000 rpm for 15 minutes, and the resulting supernatant represented the cytoplasmic component. Third, the pellet was subjected to a washing step with 500 µL of PBS. After this, it was centrifuged at 1500 ×g for 5 minutes, and the supernatant was discarded. Finally, 300 µL of 1 × sodium dodecyl sulfate (SDS) was introduced, and the liquid mixture was thoroughly mixed to yield the nuclear component. For data analysis, *GAPDH* and *U2* were selected as internal controls for the cytoplasmic and nuclear components. Additionally, to quantify the relative distribution of *SLC1A5-AS* in the cytosol and nuclei, the comparative CT ($2^{-\Delta\Delta CT}$) method was employed.

### *5′ and 3′ Rapid Amplification of cDNA Ends (RACE) Assay*

The determination of the full-length sequence of *SLC1A5-AS* was carried out using 5′ and 3′ RACE with a GeneRacer™ Kit (cat. no. L150001, Thermo Fisher, MA, USA), and all steps were performed according to the manufacturer's instructions. First, the highest-quality total RNA was prepared and verified by agarose gel electrophoresis. Subsequently, gene-specific primers (GSPs) for the target gene were meticulously designed, taking into consideration GC% and Tm values, as specified in the instructions. Total RNA was subjected to treatment with calf intestinal phosphatase (CIP) to dephosphorylate noncoding mRNA or truncated mRNA. After the RNA was precipitated, the 5′ cap structure was removed from full-length mRNA using tobacco acid pyrophosphatase (TAP). The GeneRacer™ RNA Oligo was then ligated to the 5′ ends of the dephosphorylated and decapped RNA. Next, the dephosphorylated and decapped RNA was reverse transcribed into first-strand cDNA using SuperScript™ III RT and the GeneRacer™ Oligo dT Primer. GeneRacer™ 5′ Primer and reverse GSP were used to amplify the 5′ end, while the GeneRacer™ 3′ Primer and forward GSP were used to amplify the 3′ end of *SLC1A5-AS*. In parallel, Platinum® Pfx DNA polymerase (cat. 11708-013, Thermo Fisher, MA, USA), was employed to create blunt-end PCR products for subsequent cloning into the pCR™-Blunt II-TOPO® vector (cat. no. K283020, Thermo Fisher, MA, USA). Following this, agarose gel electrophoresis and purification steps were performed to obtain the corresponding RACE products. The Zero Blunt® TOPO® PCR Cloning Kit (cat. no. K283020, Thermo Fisher, MA, USA), was utilized for TOPO cloning. Within this system, topoisomerase I facilitated the cleavage of the phosphodiester backbone after the 5′-CCCTT sequence present in the pCR™-Blunt II-TOPO® vector, allowing for covalent binding between the 3′ phosphate of the cleaved strand and the tyrosyl residue (Tyr-274) of topoisomerase I on both sides of the vector. The phospho-tyrosyl bond could then be attacked by the 5′ hydroxyl of the blunt-end PCR product, thereby reversing the reaction and releasing topoisomerase. After cloning and transformation of the relevant PCR products, approximately 10–12 clones were selected for sequencing to ensure comprehensive coverage of the 5′ and 3′ ends, with bidirectional sequencing conducted. The sequences of the gene-specific PCR primers used for 5′ and 3′ RACE analysis are provided in **Supplementary Table 2**.

### *Northern Blot*

The transcript length of *SLC1A5-AS* in Huh-7 cells was determined using a NorthernMax® Gly Kit (cat. no. AM1946, Thermo Fisher, USA), in combination with the DIG Northern Starter Kit (cat. no. 12039672910, Roche, Basel, Switzerland), with digoxin-labeled RNA probes. Here's a summary of the procedures involved: Mixed sample RNA, approximately 10 µg of enriched polyA+ RNA in each lane, was combined with an equal volume of Glyoxal Load Dye. The RNA secondary structure was denatured before agarose gel electrophoresis (prepared with DEPC water). Electrophoresis was conducted, and the process was halted when the bromophenol blue dye front had migrated almost to the bottom of the gel. Intact and high-quality RNA typically exhibited three bands corresponding to 28S, 18S, and 5S ribosomal RNA.

The RNA was transferred to a membrane using the following assembly process: paper towels were placed next to the transfer buffer reservoir. Then, three dry filter papers and two prewet filter papers were positioned on top of each other. A BrightStar-Plus membrane that had been prewetted in the transfer buffer was placed on top of the filter papers, followed by the trimmed gel. Three additional filter papers that had been prewetted in the transfer buffer were added on top of the gel. Filter paper bridges were employed on the top of the stack to bridge the stack and the transfer buffer reservoir. Ensuring the absence of bubbles between these materials was crucial. A small weight was placed on top of the device to ensure uniform contact with all stack materials. RNA was transferred from the agarose gel to a positively charged nylon membrane over a period of 2–3

hours. Overnight hybridization (lasting 14–24 hours) with probes was performed. The membrane was washed using 20 mL per 100 $cm^2$ of membrane with the wash solution. Radio-labeled blots were sealed in plastic, and the X-ray film was exposed. The PCR primers for the probes designed for *SLC1A5-AS* can be found in **Supplementary Table 2**.

### *Evaluation of the Protein-Coding Potential of SLC1A5-AS*

The protein-coding potential of *SLC1A5-AS* was assessed using the Coding Potential Assessment Tool (CPAT, http://lilab.research.bcm.edu/cpat/) and the Coding Potential Calculator (CPC, http://cpc.cbi.pku.edu.cn/). Additionally, to serve as positive controls for lncRNA, *LINK-A* (*LINC01139*) [19] and *HOTAIR* [20] were included, while *ACTB* and *GAPDH* were used as controls for protein-coding genes in these predictive analyses.

### *Ribosomal RNA-Depleted RNA Sequencing*

Mitochondrial fractions were isolated from Huh-7, Hep-3B, and PHH cells subjected to different treatments using the Mitochondria Isolation Kit for Cultured Cells as previously described. Additionally, a transient transfection strategy was employed on $5 \times 10^6$ Huh-7 cells with 75 pM of the specified small interfering RNAs (siRNAs) for 48 hours. After removing the supernatant, the cells were washed twice with PBS. Subsequently, 1 mL of PBS was added to the dish, and the cells were collected in 1.5 mL EP tubes using a cell scraper. Following centrifugation at 1500 rpm for 5 minutes at 4 °C, the supernatant was discarded, and the specified RNAs from mitochondria and Huh-7 cells were isolated using the previously described steps. RNA-seq was performed by Majorbio Biopharm Biotechnology Co., Ltd. (Shanghai, China). The transcriptome library was constructed following the TruSeqTM RNA sample preparation Kit from Illumina (cat. no. 15026495 F, San Diego, CA, USA) using 1 µg of total RNA. In summary, the polyA selection method with oligo(dT) beads was used to isolate messenger RNA exclusively, followed by fragmentation using a fragmentation buffer. Double-stranded cDNA was synthesized with random hexamer primers (Illumina) using the SuperScript double-stranded cDNA synthesis kit (Invitrogen, CA). End-repair, phosphorylation, and the addition of an 'A' base were carried out on the synthesized cDNA according to Illumina's library construction protocol. CDNA target fragments of 300 bp were selected using Low Range Ultra Agarose (2%), and DNA amplification was performed with Phusion DNA polymerase (NEB). After quantification with TBS380, an Illumina NovaSeq 6000 sequencer was used for RNA sequencing ($2 \times 150$ bp read length). For data processing, the raw sequencing reads were aligned to the human reference genome (hg38) using the splice-aware aligner HISAT2 46. Differential expression genes (DEGs) were analyzed using the DESeq2 R package (1.33.4) [21]. The *p*-values were adjusted with Benjamini and Hochberg's method to assess the false discovery rate. DEGs were defined based on adjusted $p$-values $< 0.05$ and a fold change $>1.5$ or $<0.58$.

### *Cell Proliferation Assay*

For the cell proliferation assay, cells were washed twice with PBS. Subsequently, trypsin was used to separate and disperse the cells into individual cells, and 3 mL of medium with 10% PBS was used to fully suspend the cells. The Countess 3 Automated Cell Counter (cat. no. AMQAX2000, Thermo Fisher, USA) was then employed to count the number of cells per milliliter. The cells were seeded into a flat-bottomed 96-well culture plate (cat. no. CNG3690, Corning, NY, USA) at a density of 2000 cells per well, with each well containing 100 µL of culture medium. After 24 hours of cultivation, cell viability was assessed using Cell Counting Kit-8 (CCK-8, Yeasen, Shanghai, China) assays following a 1.5-hour incubation at 37 °C. A Multiskan™ FC Microplate Photometer (cat. no. 1410101, Thermo Fisher, USA) was used to measure the absorbance at 450 nm. Each experiment was conducted with six replicates and repeated three times, with measurements taken after 1, 3, and 5 days of cultivation.

### *Invasion Assay and Migration Assay*

Cell invasion assays were conducted using FALCON chambers (cat. no. 353097, Corning, NY, USA) in triplicate, with the chambers coated with Corning® Matrigel® Matrix (cat. no. 356234, Corning, NY, USA). The migration assay followed a similar protocol, except it was performed without the Matrigel coating. In both assays, a total of 30,000–60,000 cells were seeded in a serum-free medium in the top chamber, while a medium containing 10% FBS was added to the bottom of the well to act as a chemoattractant. After 18 hours of incubation, cells on the upper membrane surface were removed using a cotton swab. The bottom membrane surface was then fixed with methanol, stained with crystal violet, and counted in five random fields using a Leica DMI4000 B automated inverted research microscope (Leica, Wetzlar and Mannheim, Germany).

### *RNA Interference*

*SLC1A5-AS* knockdown was accomplished using siRNA. The sequences of siRNA oligonucleotides targeting *SLC1A5-AS* and the negative control siRNA can be found in **Supplementary Table 2**. These siRNAs were procured from RiboBio (RiboBio Biotechnology, Guangzhou, China). Cells were transfected with Lipofectamine 2000 (cat. no. 11668019, Thermo Fisher Scientific Inc, USA) in Opti-MEM Reduced Serum Medium, with 75 pmol of siRNA. In brief, siRNA and Lipofectamine 2000 were first separately incubated with Opti-MEM Reduced Serum Medium for 10 minutes. They were then combined and allowed to incubate for an additional 10 minutes, and the mix-

ture was gently added to the culture dish. After 6 hours of incubation, the supernatant was removed, and a fresh medium containing 10% PBS was added to the dish. After 48 hours of transfection, RNA was isolated using the method described previously.

### *Generation of Lentiviral Particles and Construction of Stable Expression Cell Model*

The full-length *SLC1A5-AS* was synthesized by RiboBio Biotechnology. Primers with homologous arms designed to amplify the full-length *SLC1A5-AS* and the pWPXL vector were obtained using Primer Premier 5. Polymerase chain reaction (PCR) was employed to generate the DNA fragment, and the pWPXL vector was digested using MluI and NdeI at 37 °C for 1 hour. To create pWPXL-*SLC1A5-AS*, the human *SLC1A5-AS* sequence was seamlessly assembled into the MluI and NdeI sites of the lentivirus expression vector pWPXL (cat. no. CU201-02, Transgene, Beijing, China). Subsequently, the resulting products were transformed into competent cells (cat.no. CD201-01, Transgene, Beijing, China) and verified through agarose gel electrophoresis and sequencing in accordance with the provided instructions. The PCR primers can be found in **Supplementary Table 2**. For the transfection, pWPXL-*SLC1A5-AS*, the packaging and envelope plasmids psPAX2 (cat. no. 12260, Addgene, USA), and pMD2.G (cat. no. 12259, Addgene, USA) were introduced into HEK293T cells using Lipofectamine 2000 (Invitrogen) as an intermediary following the manufacturer's instructions. Virus particles were harvested 48 hours after transfection. HCC cells were infected with recombinant lentivirus transducing units after treatment with 1 μg/mL polybrene (Beyotime Biotechnology, Shanghai, China) to enhance infection efficiency. During the cell model cultivation, 2 μg/mL puromycin (cat. no. ST551, Beyotime Biotechnology, Shanghai, China) was added to the medium to eliminate other cells.

### *In Vivo Assays*

Male NOD-*Prkdc*$^{scid}$*Il2rg*$^{em1}$/Smoc (M-NSG) severely immunodeficient mice and male athymic BALB/c nude mice, aged 4–5 weeks old, were procured from the Shanghai Model Organisms Center, Inc. (Shanghai, China). In each group, 10 mice were subcutaneously injected with a 0.1 mL cell suspension containing $5 \times 10^6$ cells from either the pWPXL-VECTOR or pWPXL-*SLC1A5-AS* stable Huh-7 cell line. Tumor growth rates were closely monitored once solid tumors became observable. Tumor growth was assessed every other day, and its volume was calculated using the formula volume = length $\times$ width$^2$ $\times$ 0.5. The sample size was not pre-determined for these experiments. To establish the tail vein injection mouse model, separate groups of BALB/c nude mice (n = 6) were injected with $5 \times 10^5$ Huh-7 cells stably expressing either pWPXL or pWPXL-*SLC1A5-AS*. After a ten-week period, the mice were humanely euthanized, and their lung and liver tissues were extracted. Lung and liver tissues were fixed in 4% paraformaldehyde and embedded in paraffin. Following the binocular microscope examination, tissue samples were stained with hematoxylin and eosin (H&E) (Yeasen Biotechnology, Shanghai) and assessed for the number of metastatic foci in the lung and liver. To quantify the H&E staining results, the number of metastatic foci was counted across ten sections for each mouse under the microscope, and the final numbers were averaged and subjected to statistical analysis. Euthanasia of the mice was performed by placing them in a container filled with $CO_2$ at a rate of 30% chamber volume per minute. All experiments were conducted in compliance with the relevant institutional and national guidelines and regulations set forth by the Shanghai Medical Experimental Animal Care Commission.

### *Western Blot*

The cells were lysed using RIPA buffer from Beyotime Biotechnology, which contained protease inhibitors, on ice for 30 minutes. Subsequently, the lysate was centrifuged at 12,000 $\times$g for 15 minutes. The supernatant was denatured in 5$\times$ loading buffer at 100 °C for 10 minutes and separated by 10% polyacrylamide gel electrophoresis (PAGE). PAGE was conducted at 80 V until the sample migrated to the boundary between the stacking gel and the separating gel. Following this, PAGE was continued at 120 V until the loading buffer had run out from the bottom of the separating gel. Proteins within the polyacrylamide gel were transferred to a nitrocellulose filter membrane (negative control (NC) membrane) at 270 mA for 90 minutes and then blocked with 5% skim milk for 1 hour. Subsequently, the NC membrane was washed three times in TBST, with each wash lasting 10 minutes, and it was incubated with the relevant primary antibody diluted in 5% skim milk at 4 °C overnight. Afterward, the NC membrane was washed three times in TBST (10 minutes each time) and then incubated with the corresponding secondary antibody, diluted in 5% skim milk, for 1 hour at room temperature. Finally, the NC membrane was washed three times in TBST (10 minutes each time) and visualized using chemiluminescence with Super ECL Detection Reagent (Yeasen Biotechnology, Shanghai). Grayscale measurements and data statistics were conducted as follows: Bands were imported into Image J software (Version 2020, National Institutes of Health, Bethesda, MD, USA) and converted into grayscale images. The background was subtracted from the images, and the measurement parameters were set. Grayscale values of the bands were measured, and statistical analysis was performed. The target protein was normalized using the grayscale values of the internal reference protein, and graphs were created using GraphPad Prism software (version 8.0.2, GraphPad Software, Inc., San Diego CA, USA). The antibodies used are listed in **Supplementary Table 3**.

### *Glutamine Assay*

The measurement of glutamine levels was carried out using the Glutamine Microplate Assay Kit from Absin Bioscience Inc. (Shanghai, abs580185). The process began with sample preparation, where cells and medium were collected separately, with direct treatment of glutamine in the medium. Subsequently, an assay buffer was added to the cell samples, which were then sonicated for optimal suspension maintenance. After sonication, the samples were centrifuged at 8000 ×g for 10 minutes at 4 °C to obtain the supernatant. Following this, samples were processed in conjunction with control groups, where the appropriate components, such as sample or distilled water, Reaction Buffer I, and the enzyme, were mixed and incubated. The stop solution was later added to each tube and mixed, followed by a 5-minute centrifugation at 8000 ×g. The microplate setup included the organization of the sample, control, standard, and blank groups. Each of these groups had specific components added and mixed in a microplate. Absorbance was then measured at 420 nm, utilizing the standard curve for reference. Data analysis involved the application of a formula to calculate the concentration of glutamine in the samples. This detailed procedure enabled the quantification of glutamine levels in the provided samples, with meticulous precision in handling and analysis.

The formula used is noted below:

$$\begin{aligned}\text{Gln}\ (\mu\text{mol}/10^4) = (C_{\text{Standard}} \times V_{\text{Standard}}) \times (OD_{\text{Sample}} - OD_{\text{Control}}) \\ \div (OD_{\text{Standard}} - OD_{\text{Blank}}) \div (V_{\text{Sample}} \times N/V_{\text{Assay}}) \times 2 = \\ 9 \times (OD_{\text{Sample}} - OD_{\text{Control}}) \div (OD_{\text{Standard}} - OD_{\text{Blank}}) \div N\end{aligned}$$

N: the number of cells.

### *Luciferase Assay*

The experiments conducted adhered to the guidelines provided by the Pierce® Firefly Luciferase Glow Assay Kit (cat. no. 16177, Thermo Fisher, USA). For the luciferase reporter plasmids, specific fragments of the target promoter were inserted into the upstream region of the luciferase gene sequence, and expression plasmids for the transcription factor (TF) of interest were also constructed. In preparation for the experiments, Huh-7 and Hep-3B cells were seeded in 96-well plates at a density of $1 \times 10^4$ cells per well. These cells were cultured overnight at 37 °C in a 5% $CO_2$ environment. The following day, the luciferase reporter plasmids of the *SLC1A5* promoter and the promoter-mutated reporter plasmids were transfected into the cells with *MZF1* knockdown or overexpression, using Lipo2000 as per the manufacturer's instructions. The cells were then incubated for 48 hours in a constant temperature incubator. After this incubation period, the cells were washed once with PBS, and the supernatant was discarded. Cell lysis was carried out with 1× cell lysis buffer (100 µL per well), and this mixture was shaken for 15–30 minutes to ensure complete lysis. For the luciferase assay, 10 µL of the cell lysate was added to an opaque 96-well plate, followed by the addition of 50 µL of the working solution. After a 10-minute incubation period, the signal output at a 613 nm wavelength was detected. For clarity, the sequences of the primers used for cloning the *SLC1A5* promoter and the *MZF1* siRNAs can be found in **Supplementary Table 2**.

### *Chromatin Immunoprecipitation (ChIP) Assay*

The ChIP procedures were meticulously conducted in accordance with the guidelines provided by the MAGnify™ Chromatin Immunoprecipitation System (cat. no. 492024, Thermo Fisher, USA). To begin, we initiated the process by adding 100 µL of pre-cooled dilution buffer to a centrifuge tube, thoroughly mixing it with 10 µL of fully resuspended Dynabeads® Protein A/G. Next, 1 µg of the ChIP antibody and an equivalent amount of rabbit IgG antibody, used as a negative control, were placed in separate tubes and gently rotated for 1 hour at 4 °C. Simultaneously, Huh-7 cells, with a count of $2 \times 10^5$ cells per sample, were transferred to a tube, and the total volume was adjusted to 500 µL with PBS. To initiate the crosslinking of DNA-protein complexes, 13.5 µL of 37% formaldehyde was introduced to the tube, followed by a 10-minute incubation at room temperature. This crosslinking reaction was halted by the addition of 57 µL of 1.25 M glycine for 5 minutes. Following two washes with 500 µL of pre-cooled PBS, the cells were resuspended in Lysis Buffer with protease inhibitors (50 µL Lysis Buffer per $1 \times 10^6$ cells) and left on ice for a minimum of 5 minutes. Subsequently, we subjected the cell lysate to sonication for 16 cycles, with each cycle comprising 30 seconds on and 30 seconds off. The supernatant, containing chromatin fragments in the 200–500 bp range, was extracted following centrifugation at 20,000 ×g for 5 minutes at 4 °C. Per the kit's instructions, the supernatant was diluted with Dilution Buffer containing protease inhibitors. Ten microliters were reserved for the Input Control group. Following that, 100 µL of the diluted chromatin extract was combined with the beads pellet containing the specific antibody and gently mixed. The mixture was incubated at 4 °C for 2 hours. Each sample was subjected to two washes with IP Buffer 1 and IP Buffer 2. To the tube housing the beads and the 10 µL of Input Control, 54/43 µL of Reverse Crosslinking buffer containing protease K was introduced and mixed. The tubes were incubated at 55 °C for 15 minutes to reverse the crosslinking. Subsequently, the supernatant, which contained chromatin fragments and was without beads, was transferred to a new tube and incubated at 65 °C for 15 minutes, then cooled on ice for approximately 5 minutes. Finally, we purified and eluted the DNA samples as per the kit instructions, and DNA detection was performed via qPCR. For the specific primer sequences used in ChIP, please refer to **Supplementary Table 2**. Detailed information about the antibodies employed is provided in **Supplementary Table 3**.

### *RNA Pulldown*

To obtain full-length *SLC1A5-AS* DNA fragments with T7 sequences, we employed PCR using cDNA from HCC cells. Subsequently, we transcribed and labeled full-length *SLC1A5-AS* and antisense-*SLC1A5-AS* RNAs with T7 polymerase (Roche, Basel, Switzerland) and Biotin RNA Labeling Mix (Roche, Basel, Switzerland). Following this, the labeled RNAs were treated with RNase-free DNase I (Takara, Japan) and purified using RNA Clean & Concentrator (Zymo Research). The pre-treated biotinylated RNAs were then incubated with the respective protein extracts from Huh-7 and Hep-3B cells at 4 °C for 2 hours. They were gently mixed with 40 µL of washed streptavidin beads (Invitrogen, USA) and left to incubate on a rotator at 4 °C overnight. Subsequently, the beads were briefly washed four times with PBS buffer diluted with DEPC water. To release the proteins, 40 µL of DEPC water plus 10 µL of 5× loading buffer were added, and the mixture was denatured at 100 °C for 10 minutes. The proteins were then separated by gel electrophoresis and visualized using silver staining. Specific bands were excised for proteomics screening through mass spectrometry analysis conducted by Guangzhou Kidio Biotechnology Co., Ltd., located in Guangzhou, China. The identification of proteins was carried out by searching the human RefSeq protein database (https://www.ncbi.nlm.nih.gov/refseq/) using Mascot version 2.4.01 (Matrix Science, London, UK). For the primer sequences used for PCR of *SLC1A5-AS*, please refer to **Supplementary Table 2**.

### *Data Analysis and Statistics*

In the statistical analyses, GraphPad Prism 8.0.2 was the software used. A *T*-test was employed to analyze *SLC1A5-AS* and *SLC1A5* mRNA levels in paired HCC and normal tissues, as the data constituted continuous variables and met the criteria of a normal distribution. To investigate the correlation between *SLC1A5-AS* mRNA levels and overall survival, the log-rank Mantel-Cox test was performed. The presentation of data was in the form of mean values accompanied by the standard deviation (SD). These data were subjected to one-way ANOVA or independent sample *t*-tests to evaluate the distinctions among different treatment groups. The threshold for statistical significance was established at $p < 0.05$. The figures were constructed using Adobe Illustrator (version CC 2019, Adobe, Inc., San Jose, CA, USA).

## Results

### *Screening of Differentially Expressed Mitochondrial-Associated LncRNAs under Hypoxia Treatment in HCC Cells*

To identify differentially expressed oncogenic lncRNAs within the mitochondria of HCC cells under hypoxic conditions, a series of experimental steps were carried out. First, PHH and two HCC cell lines (Huh-7 and Hep-3B) were subjected to a 12-hour serum-free starvation period, followed by the addition of 200 µM $CoCl_2$ to mimic a hypoxic microenvironment, with successful modeling confirmed by the presence of key hypoxia-associated markers (*GLUT1*, *CA9*, *PDK1*, and *HIF-1α*) [17] (**Supplementary Fig. 1A–D**). Mitochondrial RNA was then isolated from the different groups after $CoCl_2$ treatment for 0, 6, and 12 hours for ribosomal RNA-depleted RNA sequencing (RNA-seq) (Fig. 1A), and the quality and efficiency of mitochondrial isolation were validated (**Supplementary Fig. 2A–D**). Subsequently, a screening process was performed to identify oncogenic mitochondria-associated lncRNAs, using the criteria of $Log_2$(Fold Change) >5 (Wilcoxon Test <0.01) when comparing Huh-7 and Hep-3B cells with PHH cells (Fig. 1B). Following this, the RNA levels of the selected lncRNAs were validated in 67 pairs of HCC and corresponding adjacent non-tumor liver tissues (Cohort 1). Out of these lncRNAs, four were significantly upregulated in HCC tissues, including *CTB-147N14.6*, *RP11-37C7.1*, *RP11-395I14.2*, and *CTB-12A17.3* (Fig. 1C). *CTB-147N14.6* exhibited the most significant increase in RNA levels ($p < 0.0001$) in HCC tissues and was identified to have a single transcript in the UCSC database (University of California, Santa Cruz, human genome GRCh38/hg38). Consequently, *CTB-147N14.6* (ENSG00000275719.1) was selected for further investigation.

### *CTB-147N14.6 is an Oncogenic Antisense LncRNA that is Correlated with Poor Prognosis in HCC Patients*

The information available in the UCSC database revealed that *CTB-147N14.6* is situated on chromosome 19q13.32 and exhibits a robust lysine 27 on histone H3 (H3K27) acetylation signal within its promoter region. Additionally, it partially overlaps in an antisense manner with the human protein-coding gene *SLC1A5* in the human genome (Fig. 2A). Consequently, it was subsequently renamed as SLC1A5-Antisense (*SLC1A5-AS*). A series of experiments and analyses confirmed several key characteristics of *SLC1A5-AS*. Notably, it was found to be a stable transcript with a length of 1229 nucleotides in the Huh-7 cell line, which allowed for successful overexpression and knockdown (Fig. 2B). RACE assays and sequencing results corroborated the precise sequence of *SLC1A5-AS* (Fig. 2C). Computational tools CPC and CPAT both indicated that *SLC1A5-AS* lacks the potential to encode proteins or small peptides (Fig. 2D). Further exploration of *SLC1A5-AS*'s subcellular localization revealed its presence in both the nucleus and cytoplasm of Huh-7 and Hep-3B cells (Fig. 2E). Furthermore, under conditions mimicking a hypoxic microenvironment achieved by $CoCl_2$ treatment, *SLC1A5-AS* RNA levels significantly increased in both Huh-7 and Hep-3B cell lines after 6 hours (Fig. 2F). Notably, the study also examined *SLC1A5-AS* RNA levels in hepatocellular car-

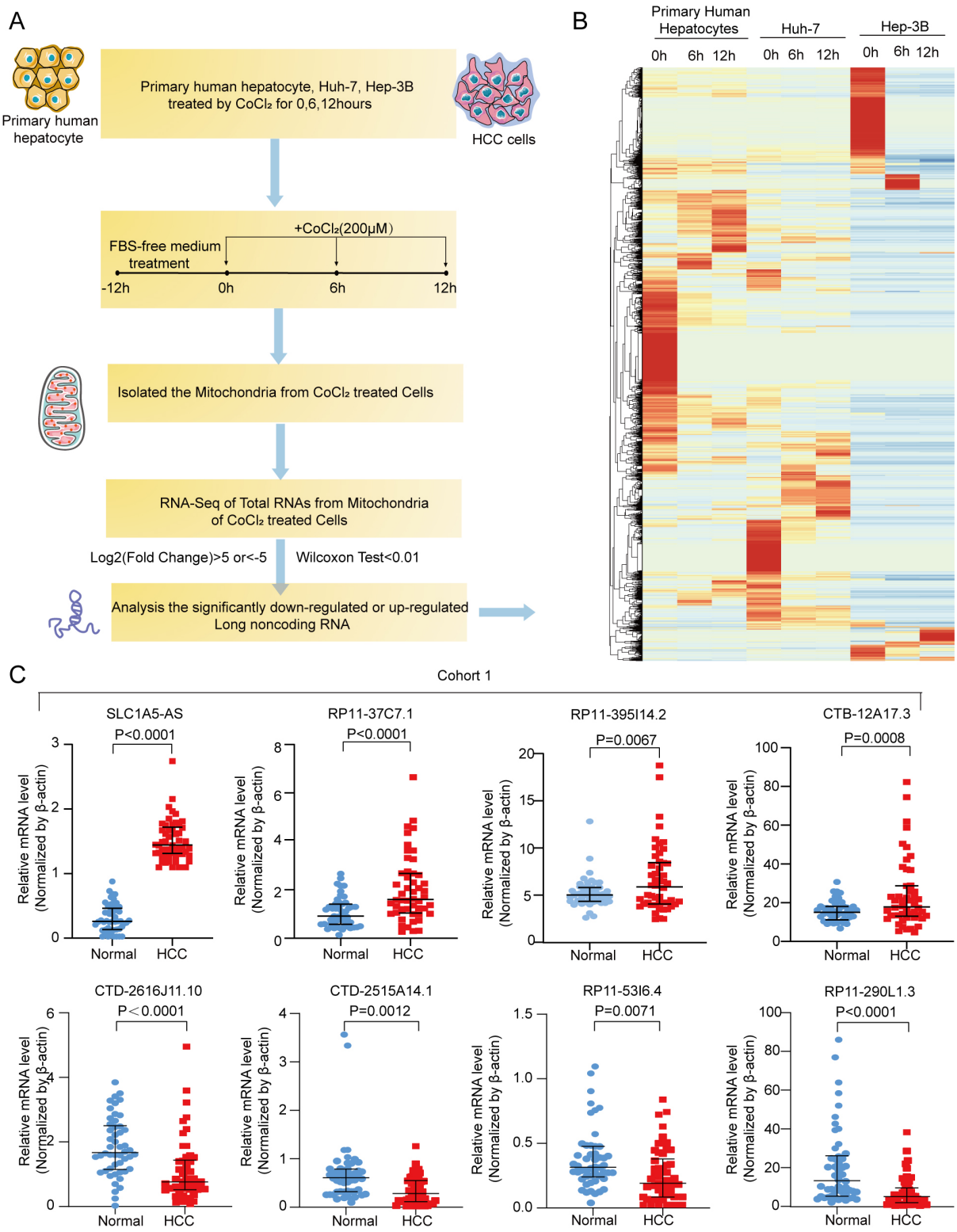


**Fig. 1. The screening process for identifying differentially expressed mitochondrial-associated long noncoding RNAs (lncRNAs) under Cobalt Chloride ($CoCl_2$) treatment in hepatocellular carcinoma (HCC) cells.** (A) The flow diagram outlines the steps involved in the screening of candidate oncogenic mitochondria-associated lncRNAs in a hypoxia cell model. (B) Heatmap showing a clustering analysis of HCC RNA sequencing results from various cell groups, each row corresponds to a gene, and each column represents a sample. The color scheme indicates gene expression levels, with red denoting upregulated genes and blue representing downregulated genes. (C) The RNA levels of candidate lncRNAs were assessed in 67 pairs of HCC and adjacent non-tumor (NT) tissues through quantitative real-time polymerase chain reaction (qRT-PCR) in Cohort 1.

cinoma (HCC) tissues in different cohorts. In The Cancer Genome Atlas liver cancer (TCGA-LIHC) cohort ($p < 0.01$) (Cohort 2) and a cohort of 140 paired HCC and normal liver tissues (Cohort 3), *SLC1A5-AS* RNA levels were substantially higher in HCC tissues compared to normal liver tissues, and elevated levels of *SLC1A5-AS* correlated with poorer prognosis for HCC patients in both cohorts (Fig. 2G,H and **Supplementary Table 1)**. These findings suggest that *SLC1A5-AS* may play a significant role in the development and prognosis of HCC, particularly under hypoxic conditions.

### *SLC1A5-AS Plays a Significant Role in Promoting the Invasive, Migratory, and Proliferative Aspects of HCC Cells*

To assess its function in carcinogenesis, two distinct siRNAs were employed to effectively knock down *SLC1A5-AS* in Huh-7 and Hep-3B cells (**Supplementary Fig. 3A**). The results clearly demonstrated that the suppression of *SLC1A5-AS* significantly impeded both the migratory and invasive capabilities of these cells (Fig. 3A,B). Furthermore, a lentivirus packaging system was utilized to establish stable *SLC1A5-AS* overexpression cell lines (**Supplementary Fig. 3B**). Notably, the overexpression of *SLC1A5-AS* led to a marked increase in the migratory and invasive potential of Huh-7 and Hep-3B cells (Fig. 3C). To gain deeper insights into *SLC1A5-AS*'s role in tumor cell growth, CCK-8 assays were conducted. These assessments revealed a significant reduction in cell growth upon *SLC1A5-AS* silencing, while *SLC1A5-AS* overexpression markedly promoted cell growth in Huh-7 and Hep-3B cells (Fig. 3D,E). These combined findings underscore the potential oncogenic role of *SLC1A5-AS* in HCC.

### *SLC1A5-AS Promotes HCC Cell Proliferation and Metastasis In Vivo*

To further assess the *in vivo* impact of *SLC1A5-AS*, we conducted subcutaneous injections of stably overexpressed pWPXL-*SLC1A5-AS* Huh-7 cells into immunodeficient M-NSG mice (n = 10). This led to a substantial increase in tumor volume and weight ($p < 0.01$) in the pWPXL-*SLC1A5-AS* group, indicating that *SLC1A5-AS* promoted HCC tumorigenesis *in vivo* (Fig. 4A). We also examined its role in HCC metastasis *in vivo*. Stably overexpressed pWPXL-*SLC1A5-AS* Huh-7 cells were injected into the tail veins of BALB/c nude mice (n = 6), with an empty vector group serving as the control. After seven weeks, the mice were euthanized, and lung and liver tissues were collected. H&E staining revealed a significantly higher number of metastatic foci in the lungs of the pWPXL-*SLC1A5-AS* group compared to the pWPXL group ($p < 0.05$) (Fig. 4B). These findings underscore the oncogenic nature of *SLC1A5-AS*, which promotes HCC cell growth and enhances tumor metastasis both *in vitro* and *in vivo*.

### *SLC1A5-AS is Involved in Glutamine Metabolism and Activation of Multiple Cancer-Promoting Signaling Pathways in HCC*

To comprehensively analyze the global gene expression patterns regulated by *SLC1A5-AS* in HCC, we employed two independent siRNAs and negative control (NC) to treat Huh-7 cells, followed by RNA-sequencing. Clustering analysis of dysregulated gene expression patterns was visualized through clustering analysis, with upregulated genes represented in red and downregulated genes in green (Fig. 5A,B). Subsequent data analysis using the Kyoto Encyclopedia of Genes and Genomes (KEGG) and Gene Ontology database (GO) revealed the top six enriched signaling pathways and biological processes. These included glutamine metabolisms, mammalian target of rapamycin complex 1 (*mTORC1*) signaling pathway, L-amino acid transmembrane transporter activity, tumor necrosis factor (*TNF*) signaling pathway, nuclear factor kappa-B (*NF-κB*) signaling pathway, and erythroblastic oncogene B (*ErbB*) signaling pathway (Fig. 5C). Furthermore, the GO analysis highlighted that *SLC1A5-AS* knockdown led to significant changes in gene sets related to the regulation of intracellular signal transduction (Fig. 5D). In addition to these findings, we integrated data from multiple public databases, including the Reactome Pathway Database, Human Molecular Signatures Database (MSigDB), and TCGA-LIHC database, to further investigate the signaling pathways involving *SLC1A5-AS* in liver cancer. Our results demonstrated a strong association between higher RNA levels of *SLC1A5-AS* and the activation of specific pathways. Notably, these pathways included glutamine metabolism, the mTOR signaling pathway, and the epithelial-mesenchymal transition (EMT) signaling pathway. We validated the top-regulated genes in these pathways by qPCR in Huh-7 cells (**Supplementary Fig. 4A–N**), reaffirming the involvement of *SLC1A5-AS* in glutamine metabolism ($p < 0.05$) and cancer-promoting signaling pathways ($p < 0.01$; $p < 0.01$) (Fig. 5E). These findings emphasize the role of *SLC1A5-AS* as an oncogene in these processes.

### *SLC1A5-AS Has a Strong Positive Correlation with the SLC1A5 Gene in HCC Tissue*

Our investigation revealed that the protein-coding gene *SLC1A5* shares the same genomic location as *SLC1A5-AS* but with opposite transcriptional directions. *SLC1A5* encodes alanine-serine-cysteine transporter 2 (*ASCT2*), a $Na^+$-dependent neutral amino acid transporter primarily located in the cell membrane [22]. *ASCT2* plays a pivotal role in mediating the exchange of amino acid substrates, particularly in facilitating the uptake of glutamine by rapidly growing tumor cells [23,24]. Numerous studies have demonstrated significant upregulation of *ASCT2* expression in various cancers, including non-small cell lung cancer (NSCLC) [25], breast cancer [26], liver cancer [27], and other tumors [28] is closely associated with

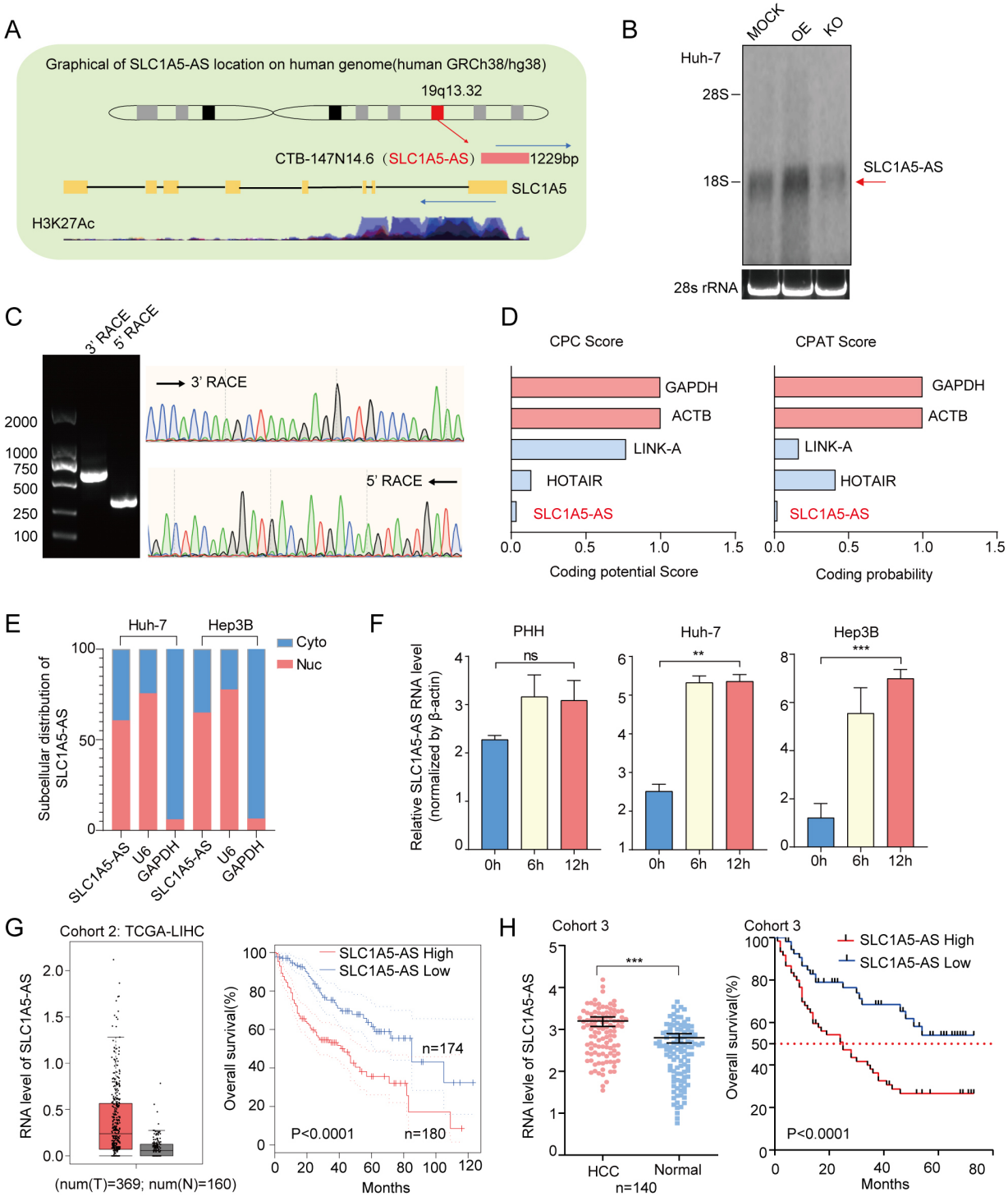


**Fig. 2.** ***Solute carrier family 1 member 5 antisense lncRNA (SLC1A5-AS)* is an oncogenic antisense lncRNA and is correlated with poor prognosis of HCC patients.** (A) *SLC1A5-AS*, previously named *CTB-147N14.6*, is located on human chromosome 19q13.32 and partly overlaps in an antisense manner with the protein-coding gene *SLC1A5*. (B) Northern blot assay in Huh-7 cells. (C) The sequence of *SLC1A5-AS* in Huh-7 cells was validated through a 5′ rapid amplification of cDNA ends (RACE) and 3′ RACE assay. (D) Computational analyses using Coding Potential Calculator (CPC) and Coding Potential Assessment Tool (CPAT) online tools. (E) Subcellular distribution of *SLC1A5-AS* in cytoplasm and nucleus of Huh-7 or Hep 3B. (F) mRNA levels of *SLC1A5-AS* were assessed in primary human hepatocytes (PHH), Huh-7, and Hep-3B cells under normoxic and hypoxic conditions. (G,H) Expression of *SLC1A5-AS* in hepatocellular carcinoma (HCC) and normal tissues and overall survival rates of HCC patients from (G) The Cancer Genome Atlas liver cancer (TCGA-LIHC) (Cohort 2) and (H) an additional 140 patients (Cohort 3). ***$p < 0.001$, **$p < 0.01$ and "ns" means no significant difference between the two groups.

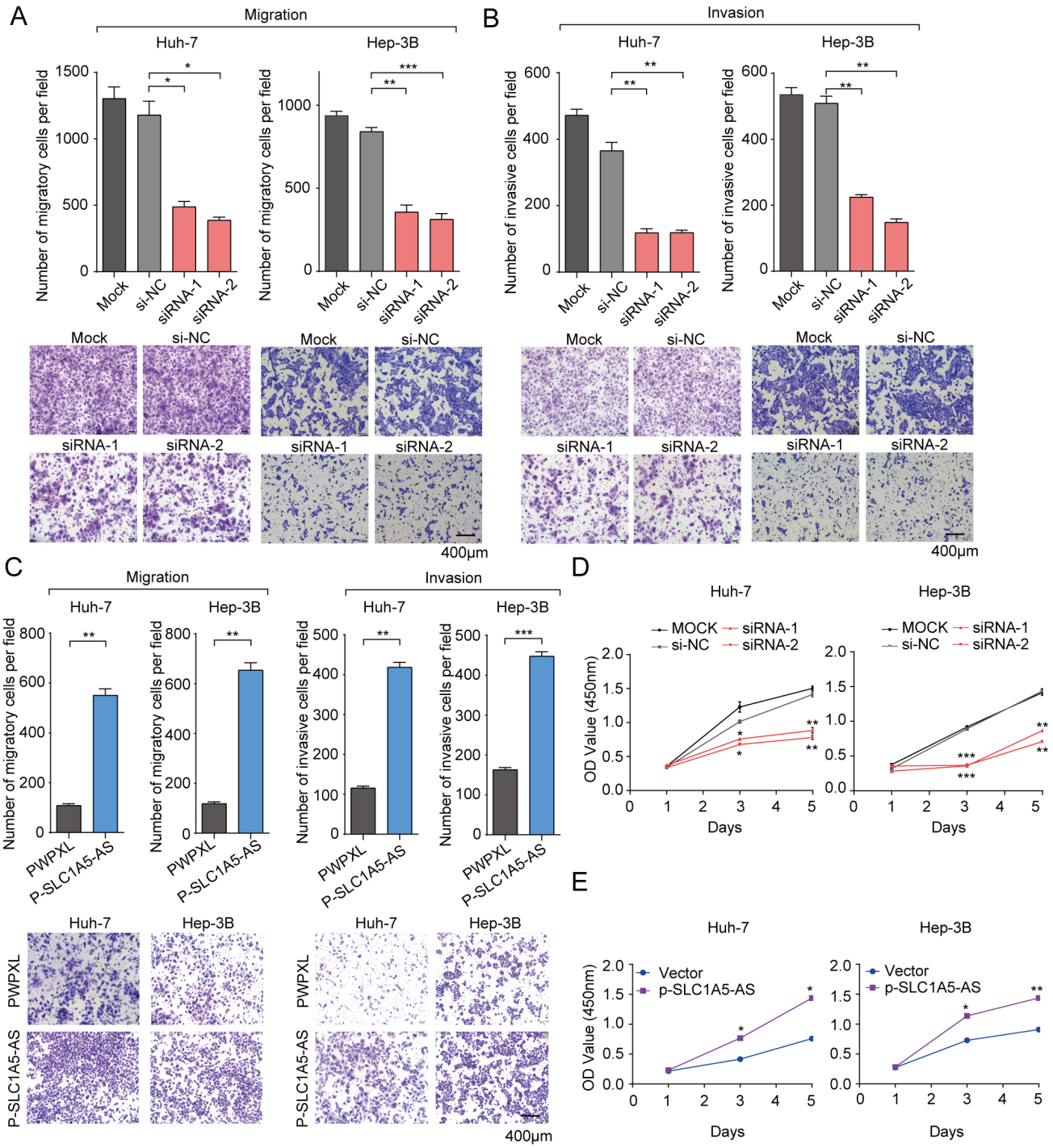


**Fig. 3. *SLC1A5-AS* promotes cell invasion, migration, and proliferation in HCC cells.** (A–C) Cell migration assay (A) and invasion assay (B) were used in *SLC1A5-AS* knockdown or overexpressed (C) Huh-7 and Hep-3B cell lines individually. Scale bar: 400 μm. (D,E) Cell proliferation among *SLC1A5-AS* knockdown (D) and overexpressed (E) Huh-7 and Hep-3B cells. The data are presented as the mean ± standard error of the mean (SEM), n = 3. Analysis using two-way ANOVA revealed statistical significance with ***$p < 0.001$, **$p < 0.01$, and *$p < 0.05$.

poor prognosis other tumors [29,30]. We also conducted an analysis of *SLC1A5* mRNA levels, copy number variations, and their association with the overall survival of liver cancer patients. The results indicated a substantial upregulation of *SLC1A5* expression in liver cancer tissues (**Supplementary Fig. 5A**). Kaplan-Meier survival curves highlighted the prognostic value ($p < 0.0001$) of *SLC1A5*, with higher expression levels correlating with poor overall and disease-specific survival ($p < 0.0036$) in liver cancer patients (**Supplementary Fig. 5B,C**). Additionally, the

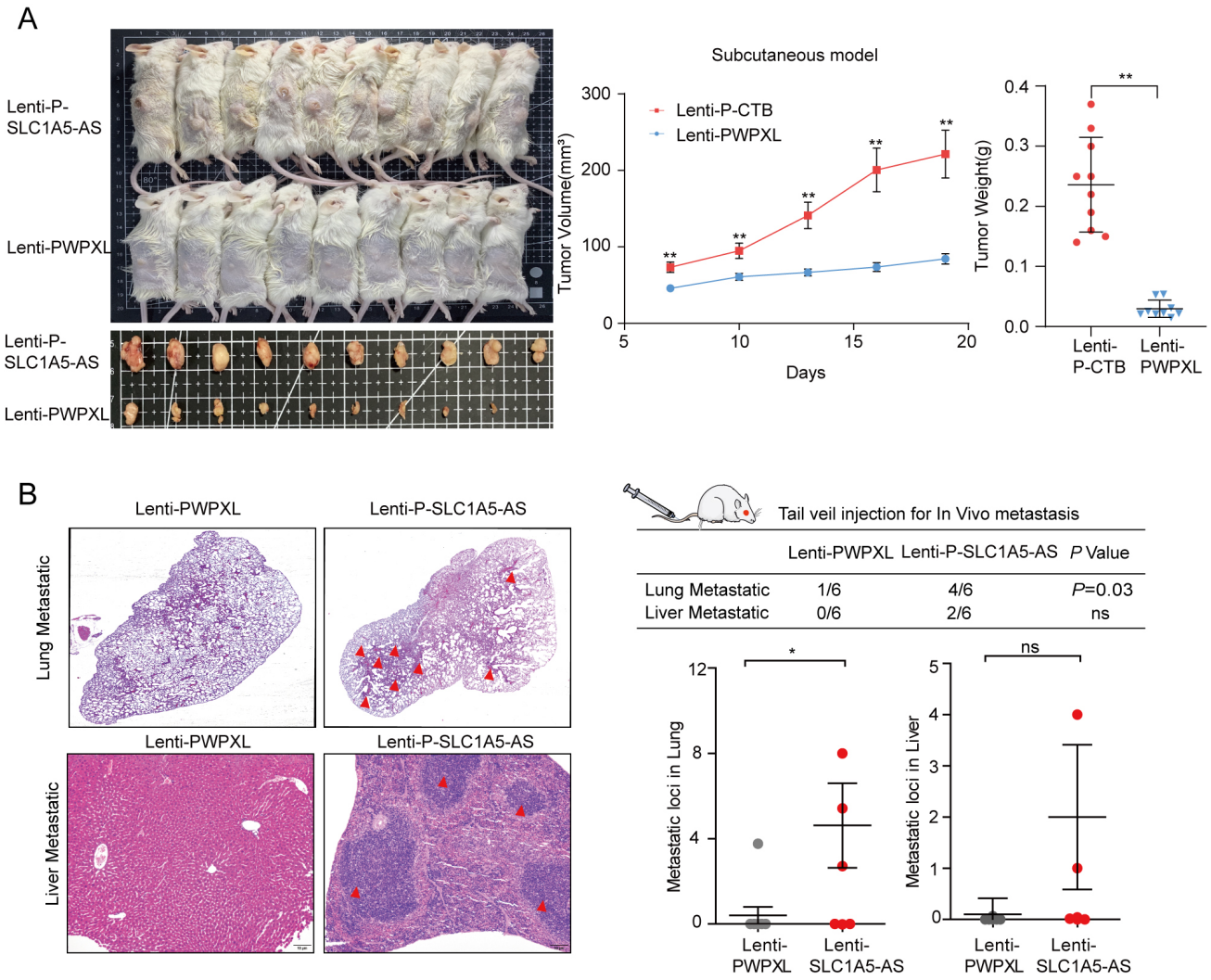


**Fig. 4. *SLC1A5-AS* promotes HCC cell proliferation and metastasis *in vivo*.** (A) Tumor volume and weight were measured in xenograft Male NOD-*Prkdc*$^{scid}$*Il2rg*$^{em1}$/Smoc (M-NSG) mouse models in both the negative control (NC) and pWPXL-*SLC1A5-AS* over-expressing groups. (B) Hematoxylin and eosin (H&E) staining statistical analysis of metastatic foci in lung and liver tissues from nude mice after tail vein injection of stable pWPXL-*SLC1A5-AS* Huh-7 cells. Scale bar: 20 μm. Red arrows indicate metastatic foci formed by Huh-7 cells. Significance levels are indicated as $^{**}p < 0.01$, $^{*}p < 0.05$, and ns, not significant ($p > 0.05$).

mRNA level of *SLC1A5* was significantly higher in stage III compared to stage I ($p < 0.05$), suggesting a positive correlation between elevated *SLC1A5* levels and the advanced stage of hepatocellular carcinoma. These findings imply that *SLC1A5* could serve as a potential molecular marker for classifying the clinical staging of HCC patients with HCC (**Supplementary Fig. 5D**). Further analysis of the correlation between *SLC1A5* expression levels and copy number amplification in genomic loci revealed a strong positive relationship. We found a strong association between genomic copy number and *SLC1A5* mRNA levels, with a confidence level of 0.95 ($p < 0.0001$, **Supplementary Fig. 5E**). *SLC1A5-AS* is located on the antisense strand of *SLC1A5*. Thus, we further validated the correlation of *SLC1A5* and *SLC1A5-AS* with the Gene Expression Profiling Interactive Analysis database (http://gepia.cancer-pku.cn/index.html). The results showed that there was no correlation between the *SLC1A5* and *SLC1A5-AS* in normal tissues, but there was a significant positive correlation in liver cancer tissues ($p < 0.0001$) (**Supplementary Fig. 5F**). The copy number of *SLC1A5-AS* in HCC was also verified in 67 paired samples, and the results revealed that *SLC1A5-AS* had significant copy number increases in HCC tissue. *SLC1A5-AS* was also the main cause of genomic instability after hypoxia, and a higher *SLC1A5-AS* genomic copy number was shown in HCC tissues ($p < 0.001$, **Supplementary Fig. 5G**). In summary, *SLC1A5* plays an oncogenic role in HCC, and *SLC1A5-AS* is positively correlated with *SLC1A5* at the RNA level, and both have significant copy number amplification at the genome loci. Therefore, we further explored whether there is a regulatory relationship between them.

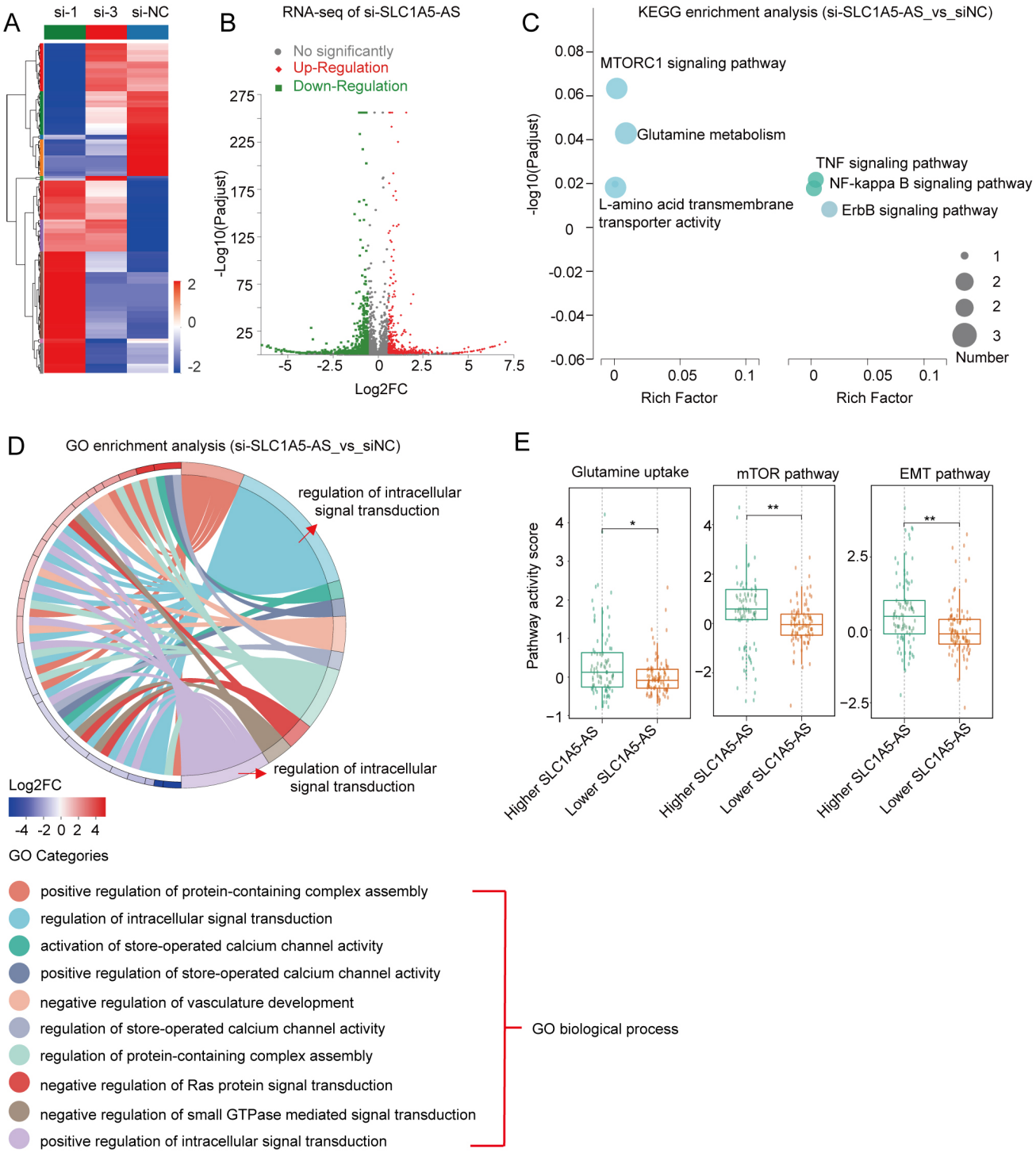


**Fig. 5. *SLC1A5-AS* is strongly correlated with glutamine metabolism and activation of multiple cancer-promoting signaling pathways in HCC.** (A) Heatmap for RNA-seq and clustering analysis in *SLC1A5-AS* knockdown Huh-7 cells. (B) Volcano plot for differential expression genes. (C,D) Kyoto Encyclopedia of Genes and Genomes (KEGG) and Gene Ontology database (GO) enrichment analysis after *SLC1A5-AS* knockdown. (E) Higher RNA level *SLC1A5-AS* contributes to the pathway activity score of glutamine uptake, mammalian target of rapamycin (mTOR) pathway and epithelial-mesenchymal transition (EMT) pathway. $^{**}p < 0.01$ and $^{*}p < 0.05$.

### *SLC1A5-AS Increases the mRNA/Protein Level of SLC1A5 and Promotes Glutamine Uptake*

In our quest to uncover the molecular mechanisms by which *SLC1A5-AS* regulates *SLC1A5*, we conducted experiments to assess the impact of *SLC1A5-AS* on *SLC1A5* expression. Following the knockdown of *SLC1A5-AS* using siRNAs in Huh-7 and Hep-3B cells, we observed a significant decrease in the mRNA levels of *SLC1A5* (Fig. 6A).

Conversely, *SLC1A5-AS* overexpression in HCC cells resulted in a marked increase in *SLC1A5* mRNA levels (Fig. 6B). These effects were mirrored at the protein level, as evidenced by decreased *SLC1A5* (*ASCT2*) protein upon *SLC1A5-AS* knockdown (Fig. 6C) and increased *SLC1A5* protein expression when *SLC1A5-AS* was overexpressed (Fig. 6D). Given the pivotal role of *SLC1A5* as a transporter in glutamine metabolism, we proceeded to investigate cellular glutamine uptake in HCC cells following *SLC1A5-AS* modulation. Silencing *SLC1A5-AS* led to significant inhibition of $^{3}$H-glutamine uptake ($p < 0.001$), whereas *SLC1A5-AS* overexpression had the opposite effect, significantly increasing $^{3}$H-glutamine uptake ($p < 0.001$) (Fig. 6E). Considering that *ASCT2* has been identified as a therapeutic target in various cancer types, we tested two *ASCT2* inhibitors in Huh-7 cells. Our results demonstrated a substantial reduction in glutamine uptake ($p < 0.001$) upon knocking down both *SLC1A5-AS* and *SLC1A5*. Strikingly, the same effect on glutamine uptake was observed when using *ASCT2* inhibitors ($p < 0.01$) (Fig. 6F). These findings collectively underscore the potential of *SLC1A5-AS* as an effective target for intervening in glutamine metabolism, making it a promising avenue for therapeutic intervention in cancer.

### *SLC1A5-AS Acts as a Molecular Decoy by Directly Binding with MZF1 at the Promoter Region of SLC1A5*

To unravel the specific molecular mechanism underlying the regulation of *SLC1A5* expression by *SLC1A5-AS*, we conducted an RNA pulldown assay to identify proteins that interact with *SLC1A5-AS* in HCC cells. We visualized the polyacrylamide gel bands using silver staining (Fig. 7A) and selected bands highly enriched in the sense group. Mass spectrometry analysis revealed several proteins that can specifically bind to *SLC1A5-AS* (Fig. 7B). Additionally, we predicted the transcription factors binding to the *SLC1A5* promoter region using the JASPAR online tool (https://jaspar.genereg.net/). Surprisingly, we found that *MZF1*, identified by mass spectrometry, can also directly bind to the promoter region of *SLC1A5*, as predicted by JASPAR (Fig. 7C and **Supplementary Fig. 6A**). We investigated the correlations of transcription factors and *SLC1A5* in both HCC and normal tissues (**Supplementary Fig. 6B** and **Supplementary Fig. 7**). Subsequently, we confirmed the interaction between *SLC1A5-AS* and *MZF1* in Huh-7 and Hep-3B cell lines through an RNA pulldown assay followed by Western blotting (Fig. 7D). *MZF1* is a zinc finger transcription factor known to suppress the expression of target genes, acting as a tumor suppressor in previous studies [31,32]. Here, we observed that *MZF1* was significantly downregulated in HCC tissues ($p < 0.05$) (**Supplementary Fig. 8**) and had a strong correlation with the mRNA level of *SLC1A5* in HCC (**Supplementary Fig. 6B**). Furthermore, we found that the binding between *MZF1* and *SLC1A5-AS* was significantly stronger under hypoxic conditions (Fig. 7E). To confirm the regulatory role of *MZF1* in the *SLC1A5-AS/SLC1A5* axis, luciferase assays in HCC cell lines (Huh-7 and Hep-3B) demonstrated that knockdown of *MZF1* increased the promoter activity of *SLC1A5*, while overexpression of *MZF1* had the opposite effect (Fig. 7F). We performed ChIP assays using an *MZF1* antibody to validate *MZF1* occupancy at the *SLC1A5* promoters in Huh-7 cells. Importantly, overexpression of *SLC1A5-AS* significantly reduced the binding of *MZF1* to the *SLC1A5* promoter sequence (Fig. 7G). Additionally, site-directed mutagenesis nullified the increased promoter activity upon *MZF1* knockdown and the decreased promoter activity in *MZF1*-overexpressing cells (Fig. 7H). The mutants also failed to respond to hypoxia-induced *SLC1A5* overexpression (Fig. 7I). In summary, our findings suggest that *SLC1A5-AS* acts as a molecular decoy by binding with *MZF1*, a negative regulator of *SLC1A5*. This interaction leads to the removal of inhibition on the *SLC1A5* promoter, ultimately promoting the expression of *SLC1A5* (Fig. 7J).

## Discussion

Mitochondria serve as energy production and metabolic hubs, intricately linked to metabolic reprogramming, a pivotal factor in cancer progression [33]. Hypoxic stress is a common feature of solid tumors [34], including HCC, prompting mitochondria to adapt metabolic pathways to support tumor cell survival and growth [5]. Tumor cells exhibit a metabolic advantage in nutrient uptake, particularly for glutamine, which is vital for amino acids, nucleotides, and lipids synthesis and contributes to mTORC1 pathway activation, driving tumor progression [24,35–37]. This preference for glutamine is widespread in cancer cells [38], highlighting the need to comprehend the intricate connection between metabolic reprogramming, mitochondria, and potential therapeutic targets in HCC.

To shed light on this interplay, we established a hypoxic cell model using PHH and two HCC cell lines (Huh-7 and Hep-3B) to investigate mitochondrial-associated lncRNAs' dysregulation in response to hypoxia. LncRNAs are non-coding transcripts with exceeding 200 nucleotides that have garnered attention for their roles in metabolic reprogramming. LncRNAs modulate glutamine metabolism and contribute to glutamine addiction by regulating key enzymes that are integral to tumor progression [25,39–42]. While many lncRNAs have been identified in response to hypoxia, research on mitochondrial-associated lncRNAs remains limited. From our screening, we identified a candidate lncRNA, *CTB-147N14.6*, whose RNA levels significantly increased under hypoxia and were strongly associated with poor prognosis in HCC patients. We subsequently renamed it *SLC1A5-AS*, recognizing its antisense nature to the protein-coding gene *SLC1A5*. *SLC1A5* encodes *ASCT2*, a sodium-dependent glutamine transporter predominantly

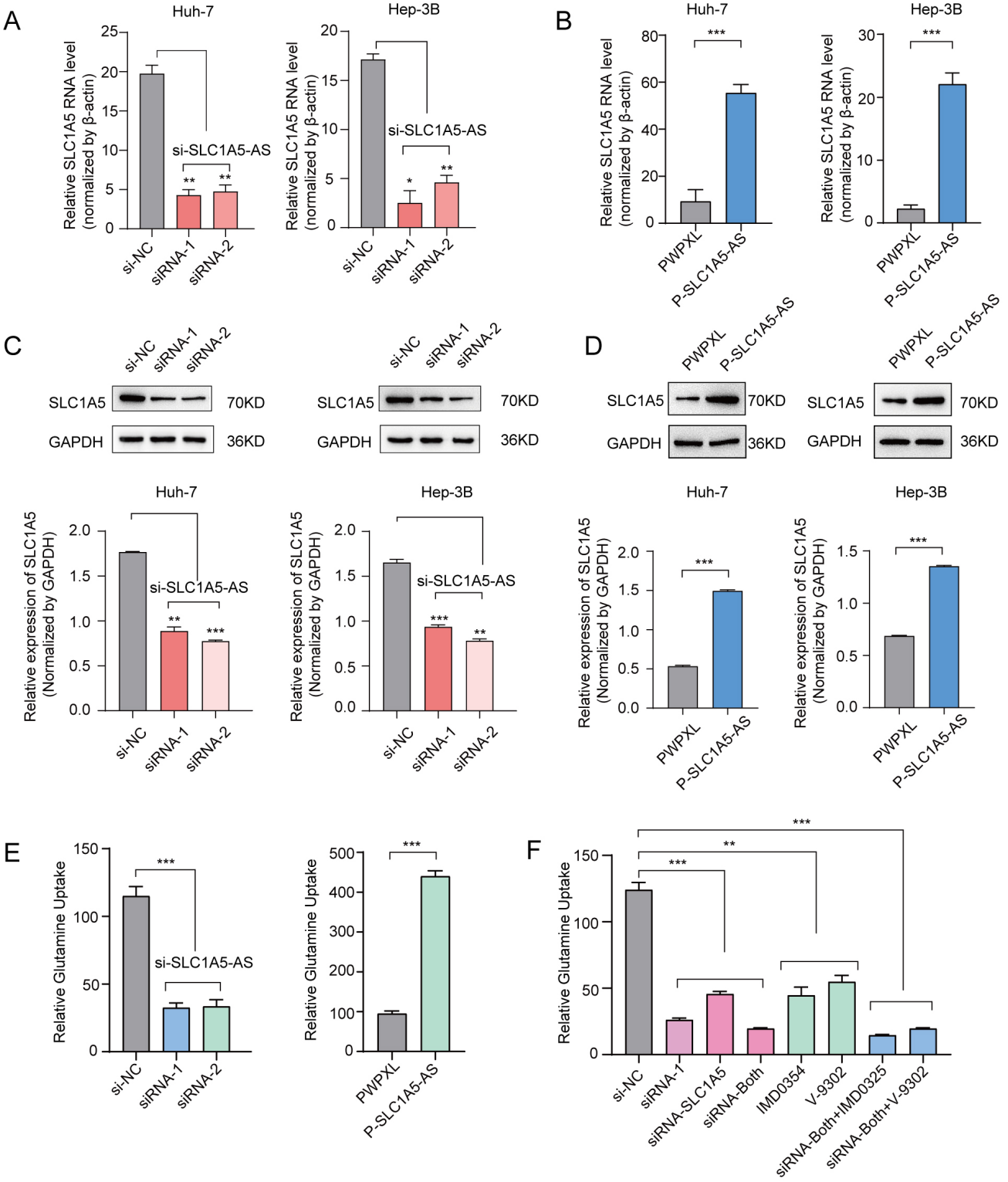


**Fig. 6. *SLC1A5-AS* increases the mRNA/protein level of *SLC1A5* and promotes glutamine uptake.** (A,B) The mRNA levels of *SLC1A5* in Huh-7 and Hep-3B cells were assessed through quantitative PCR (qPCR) after the knockdown (A) or overexpression (B) of *SLC1A5-AS*. (C,D) The protein levels of *SLC1A5* in Huh-7 and Hep-3B cells were determined by immunoblotting following the (C) knockdown or (D) overexpression of *SLC1A5-AS*. Corresponding gray value measurements and data statistics were performed. (E) Glutamine uptake was evaluated in *SLC1A5-AS* knockdown or overexpression Huh-7 cells. (F) Glutamine uptake ability was assessed following treatment with small interfering RNAs (siRNAs) or IMD0354 or V-9302 in Huh-7 cells. Data are presented as the mean ± SEM, n = 3 biologically independent experiments, analyzed using two-way ANOVA, with significance levels indicated as ***$p < 0.001$, **$p < 0.01$, *$p < 0.05$.

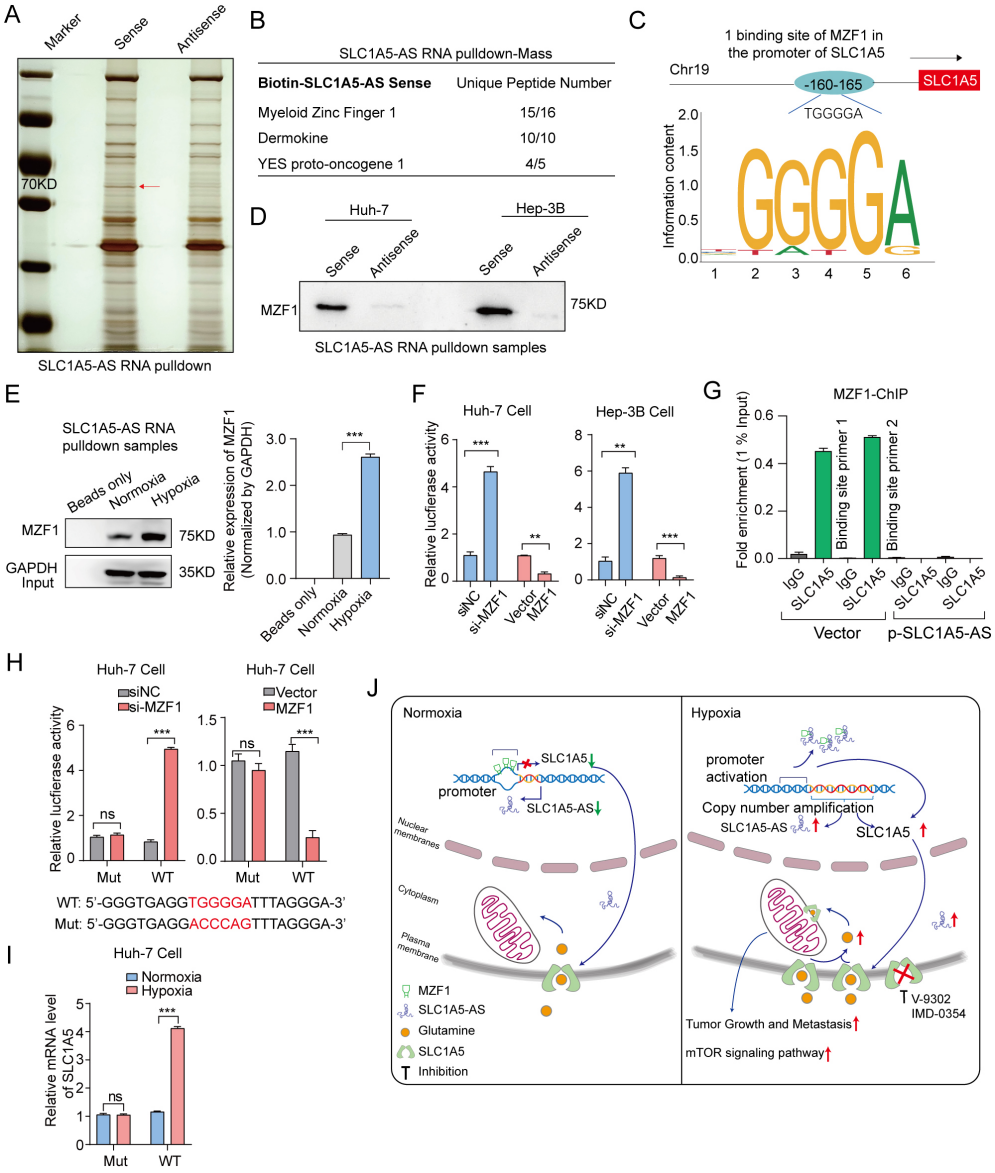


**Fig. 7. *SLC1A5-AS* promotes *SLC1A5* expression by inhibiting *myeloid zinc finger 1 (MZF1)* function.** (A) The RNA pull-down assay revealed the proteins that interacted with *SLC1A5-AS*, visualized by silver staining. The antisense group served as a control. (B) Mass spectrometry was employed to identify the proteins that are specifically bound to *SLC1A5-AS*. (C) The online tool JASPAR was utilized to predict the binding sites of *MZF1* on the promoter region of *SLC1A5*. (D) Western blotting with *SLC1A5-AS* pull-down samples validated the binding of *MZF1* and *SLC1A5-AS* in Huh-7 and Hep-3B cell lines. The antisense group was used as a negative control. (E) Western blotting with *SLC1A5-AS* pull-down samples confirmed the binding of *MZF1* and *SLC1A5-AS* in Huh-7 cells under normoxia and hypoxia conditions. Beads-only control was included. Corresponding gray value measurements and data statistics were conducted. (F) The luciferase assay was utilized to assess the promoter activity of *SLC1A5* after knockdown/overexpression of *MZF1* in Huh-7 and Hep-3B cells. (G) chromatin immunoprecipitation (ChIP)-qPCR analysis detected the binding of *MZF1* to the binding site on the *SLC1A5* promoter in the control group (vector) and *SLC1A5-AS* overexpressing Huh-7 cells. (H) The luciferase assay was used to evaluate the promoter activity of *SLC1A5* after mutation of the *MZF1* binding site in Huh-7 cells. (I) The luciferase assay was conducted under normoxia and hypoxia conditions with mutated and wide-type promoters. (J) A graphical representation of the role of the *SLC1A5-AS*/*MZF1*/alanine-serine-cysteine transporter 2 (*ASCT2*) axis in malignant progression in HCC. In summary, *SLC1A5-AS*, an antisense lncRNA of *SLC1A5*, plays a key role in promoting HCC tumorigenesis and metastasis. It does so by upregulating *ASCT2* expression through its interaction with *MZF1*, thus enhancing glutamine uptake, mTOR signaling pathway activation, and cell growth and metastasis. Silencing *SLC1A5-AS* and combining it with *ASCT2* inhibitors may offer a promising therapeutic strategy for HCC treatment. Data is presented as the mean ± SEM, n = 3 biologically independent experiments, analyzed via two-way ANOVA. ***$p <$ 0.001, **$p < 0.01$, ns, not significant ($p > 0.05$).

located in the cytoplasmic membrane [43,44]. *ASCT2*, also known as *SLC1A5*, has been implicated in various cancers, contributing to glutamine addiction and tumorigenesis [23,45], often correlating with poor patient outcomes [22]. It upregulates glutamine transport, activating mTOR [24, 46], phosphatidylin-ositol-3-kinase (PI3K)/protein kinase B (AKT) [47], janus kinase 2 (JAK2)/signal transducers and activators of transcription 3 (STAT3) [48], and transforming growth factor $\beta$1 (TGF-$\beta$1)/smad family member 2/3 (SMAD2/3) [49] signaling pathways, promoting tumor growth. Therefore, targeting *SLC1A5* holds promise as a therapeutic approach in cancer treatment. To uncover the genes and molecular mechanisms regulated by *SLC1A5-AS* in HCC, we conducted RNA-Seq. KEGG and GO enrichment analyses revealed that *SLC1A5-AS* primarily participates in glutamine metabolism, L-amino acid transmembrane transporter activity, and the NF-$\kappa$B signaling pathway, mirroring the pathways involving *SLC1A5*. Furthermore, we established a strong correlation between *SLC1A5-AS* and *ASCT2* in HCC tissues, indicating that *SLC1A5-AS* effectively regulates *ASCT2* mRNA and protein levels in HCC cells. To validate the role of *SLC1A5-AS* in glutamine metabolism, we measured glutamine uptake capacity in Huh-7 cells upon *SLC1A5-AS* knockdown and overexpression. The results demonstrated that altering *SLC1A5-AS* expression significantly impacted glutamine uptake in Huh-7 cells. At present, emerging inhibitors, including IMD-0354, which disrupts the plasma membrane localization of SLC1A5 [50] and V-9302, which decreases glutamine transport and metabolism [51], have reached the preclinical phase. We tested these inhibitors in combination with si-*SLC1A5* and si-*SLC1A5-AS* in Huh-7 cells, revealing that they all significantly reduced glutamine uptake, with the combined approach yielding the most substantial reduction. Given that *SLC1A5-AS* silencing mimics the effects of *SLC1A5* inhibitors on glutamine uptake, *SLC1A5-AS* emerges as a prospective therapeutic target for curtailing glutamine metabolism in tumor cells. To uncover the mechanism of *SLC1A5-AS* in regulating *SLC1A5* mRNA levels in HCC cells, we conducted a biotinylated *SLC1A5-AS* RNA pulldown assay to identify candidate binding proteins. Strikingly, *MZF1* exhibited strong binding to the *SLC1A5* gene promoter region. We further validated the interaction between *SLC1A5-AS* and *MZF1* in HCC cell lines, demonstrating that *MZF1* knockdown increased *SLC1A5* promoter activity, while *MZF1* overexpression produced the opposite effect. *MZF1* belongs to the zinc finger transcription factor family, featuring a SCAN domain family of zinc finger proteins (SCAN-ZFP) [52]. By binding to gene promoter regions, *MZF1* can regulate transcription and exert epigenetic control over diverse biological processes [53]. *MZF1* has been shown to play a crucial role in controlling proliferation, metastasis, and invasiveness in various cancers [54,55]. Chromatin immunoprecipitation experiments further confirmed the interaction between *MZF1* and the *SLC1A5* promoter, which was impaired by *SLC1A5-AS* overexpression. Notably, hypoxia intensified *MZF1*'s binding to *SLC1A5-AS*, strengthening the connection.

## Conclusions

Our findings revealed that the lncRNA *SLC1A5-AS*, situated at the 19q13.32 locus, exhibits a partial reverse complementary sequence with the glutamine transporter *SLC1A5*. Notably, *SLC1A5-AS* functions as an oncogene, actively promoting the proliferation and metastasis of HCC cells both *in vitro* and *in vivo*. This pro-oncogenic role is attributed to its capacity to enhance glutamine uptake through elevating *ASCT2* protein levels, thereby contributing to the progression of HCC. Furthermore, the upregulation of *SLC1A5* expression, orchestrated by *SLC1A5-AS*, hinges on its role as a molecular decoy for *MZF1*. By sequestering *MZF1*, *SLC1A5-AS* impedes its ability to inhibit *SLC1A5* promoter activity. Consequently, *SLC1A5-AS* emerges as a promising prognostic indicator, and its combination with *ASCT2* inhibitors holds the potential to be an effective therapeutic approach for HCC. A comprehensive comprehension of the *SLC1A5-AS*/*MZF1*/*ASCT2* axis can significantly enrich our understanding of HCC progression and pave the way for advanced cancer screening and precision therapy.

## Availability of Data and Materials

The authors declare that all relevant data of this study are available within the article or from the corresponding authors on reasonable request. Most of the data that supports the findings of this study are available in the supplementary material of this article.

## Author Contributions

Conceptualization, ZL, and JW; Methodology, ZL, JWJ, WD, RCZ, JW, WZ, QW, RYW, HW, HD and RCZ; Validation, ZL, JWJ, WD, JW, WZ, QW, RYW and JXW; Formal analysis, ZL, JWJ, WD, RCZ, JW, WZ, QW, RYW, HW, HD and JXW; Investigation, ZL, WD, RCZ and JWJ; Resources, ZL, JW, WD, RCZ and HD; Data curation, ZL, JWJ, JW, HD, RCZ and HW; Original draft preparation, ZL, JWJ, WD, RCZ, JW, WZ, QW, RYW, HW, HD and JXW; Funding acquisition, ZL, JW, WD, HD and RCZ. All authors have agreed to publish the final version of the manuscript, take responsibility for all aspects of the work and ensure the accuracy or completeness of any part of the work.

## Ethics Approval and Consent to Participate

All methods were carried out abiding by relevant guidelines and regulations. All experimental protocols of animals were approved by the Ethics Committee of Shang-

hai University (Ethical approval number: ECSHU 2023-004) and experimental protocols of humans were approved by the Second Military Medical University (Ethical approval number: 2020-035-02). Informed consent was obtained from all subjects. All animal experimental methods are reported in accordance with ARRIVE guidelines for the reporting of animal experiments. Human experimentation is consistent with the Declaration of Helsinki.

## Acknowledgment

Not applicable.

## Funding

This work was supported by grants from the National Natural Science Foundation of China (81802810); The National Key Research and Development Program of China (2020YFA0113000, 2018YFA0109800); Basic Research Program of Shanghai (20JC1412200); Shanghai Municipal Health Commission (20214Y0359); Shanghai Science and Technology Administration Commission (22Y11909100).

## Conflict of Interest

The authors declare no conflict of interest.

## Supplementary Material

Supplementary material associated with this article can be found, in the online version, at https://doi.org/10.24976/Discov.Med.202335179.96.

## References

[1] Sung H, Ferlay J, Siegel RL, Laversanne M, Soerjomataram I, Jemal A, *et al*. Global Cancer Statistics 2020: GLOBOCAN Estimates of Incidence and Mortality Worldwide for 36 Cancers in 185 Countries. CA: a Cancer Journal for Clinicians. 2021; 71: 209–249.

[2] Reig M, Forner A, Rimola J, Ferrer-Fàbrega J, Burrel M, Garcia-Criado Á, *et al*. BCLC strategy for prognosis prediction and treatment recommendation: The 2022 update. Journal of Hepatology. 2022; 76: 681–693.

[3] Jing X, Yang F, Shao C, Wei K, Xie M, Shen H, *et al*. Role of hypoxia in cancer therapy by regulating the tumor microenvironment. Molecular Cancer. 2019; 18: 157.

[4] Bao MHR, Wong CCL. Hypoxia, Metabolic Reprogramming, and Drug Resistance in Liver Cancer. Cells. 2021; 10: 1715.

[5] Schito L, Rey S. Cell-Autonomous Metabolic Reprogramming in Hypoxia. Trends in Cell Biology. 2018; 28: 128–142.

[6] Vyas S, Zaganjor E, Haigis MC. Mitochondria and Cancer. Cell. 2016; 166: 555–566.

[7] Kopinski PK, Singh LN, Zhang S, Lott MT, Wallace DC. Mitochondrial DNA variation and cancer. Nature Reviews. Cancer. 2021; 21: 431–445.

[8] Porporato PE, Filigheddu N, Pedro JMBS, Kroemer G, Galluzzi L. Mitochondrial metabolism and cancer. Cell Research. 2018; 28: 265–280.

[9] ENCODE Project Consortium, Birney E, Stamatoyannopoulos JA, Dutta A, Guigó R, Gingeras TR, *et al*. Identification and analysis of functional elements in 1% of the human genome by the ENCODE pilot project. Nature. 2007; 447: 799–816.

[10] St Laurent G, Wahlestedt C, Kapranov P. The Landscape of long noncoding RNA classification. Trends in Genetics: TIG. 2015; 31: 239–251.

[11] Cech TR, Steitz JA. The noncoding RNA revolution-trashing old rules to forge new ones. Cell. 2014; 157: 77–94.

[12] Rinn JL, Chang HY. Long Noncoding RNAs: Molecular Modalities to Organismal Functions. Annual Review of Biochemistry. 2020; 89: 283–308.

[13] Kopp F, Mendell JT. Functional Classification and Experimental Dissection of Long Noncoding RNAs. Cell. 2018; 172: 393–407.

[14] Yang Y, He B, Yang R, Chen D, Zhang X, Li F, *et al*. Comprehensive analysis of lncRNA expression profiles in rats with cerebral ischemia-reperfusion injury after treatment with 20(R)-ginsenoside Rg3. Journal of Integrative Neuroscience. 2022; 21: 16.

[15] Galvan DL, Green NH, Danesh FR. The hallmarks of mitochondrial dysfunction in chronic kidney disease. Kidney International. 2017; 92: 1051–1057.

[16] Sun H, Huang Z, Sheng W, Xu MD. Emerging roles of long noncoding RNAs in tumor metabolism. Journal of Hematology & Oncology. 2018; 11: 106.

[17] Zheng H, Wang N, Li L, Ge L, Jia H, Fan Z. miR-140-3p enhanced the osteo/odontogenic differentiation of DPSCs via inhibiting KMT5B under hypoxia condition. International Journal of Oral Science. 2021; 13: 41.

[18] Ibrahim AA, Schmithals C, Kowarz E, Köberle V, Kakoschky B, Pleli T, *et al*. Hypoxia Causes Downregulation of Dicer in Hepatocellular Carcinoma, Which Is Required for Upregulation of Hypoxia-Inducible Factor 1$\alpha$ and Epithelial-Mesenchymal Transition. Clinical Cancer Research: an Official Journal of the American Association for Cancer Research. 2017; 23: 3896–3905.

[19] Lin A, Li C, Xing Z, Hu Q, Liang K, Han L, *et al*. The LINK-A lncRNA activates normoxic HIF1$\alpha$ signalling in triple-negative breast cancer. Nature Cell Biology. 2016; 18: 213–224.

[20] Yang L, Peng X, Li Y, Zhang X, Ma Y, Wu C, *et al*. Long non-coding RNA HOTAIR promotes exosome secretion by regulating RAB35 and SNAP23 in hepatocellular carcinoma. Molecular Cancer. 2019; 18: 78.

[21] Love MI, Huber W, Anders S. Moderated estimation of fold change and dispersion for RNA-seq data with DESeq2. Genome Biology. 2014; 15: 550.

[22] Liu Y, Zhao T, Li Z, Wang L, Yuan S, Sun L. The role of ASCT2 in cancer: A review. European Journal of Pharmacology. 2018; 837: 81–87.

[23] Jiang H, Zhang N, Tang T, Feng F, Sun H, Qu W. Target the human Alanine/Serine/Cysteine Transporter 2(ASCT2): Achievement and Future for Novel Cancer Therapy. Pharmacological Research. 2020; 158: 104844.

[24] van Geldermalsen M, Wang Q, Nagarajah R, Marshall AD, Thoeng A, Gao D, *et al*. ASCT2/SLC1A5 controls glutamine uptake and tumour growth in triple-negative basal-like breast cancer. Oncogene. 2016; 35: 3201–3208.

[25] Liu Y, Ge X, Pang J, Zhang Y, Zhang H, Wu H, *et al*. Restricting Glutamine Uptake Enhances NSCLC Sensitivity to Third-Generation EGFR-TKI Almonertinib. Frontiers in Pharmacology. 2021; 12: 671328.

[26] Zhou P, Liang X, Zhou C, Qin J, Hou C, Zhu Z, *et al*. Glutamine-$\beta$-cyclodextrin for targeted doxorubicin delivery to triple-negative breast cancer tumors via the transporter ASCT2. Journal of Materials Chemistry. B. 2019; 7: 5363–5375.

[27] Du D, Liu C, Qin M, Zhang X, Xi T, Yuan S, *et al*. Metabolic dysregulation and emerging therapeutical targets for hepatocel-

lular carcinoma. Acta Pharmaceutica Sinica. B. 2022; 12: 558–580.

[28] Najumudeen AK, Ceteci F, Fey SK, Hamm G, Steven RT, Hall H, *et al*. The amino acid transporter SLC7A5 is required for efficient growth of KRAS-mutant colorectal cancer. Nature Genetics. 2021; 53: 16–26.

[29] Shimizu K, Kaira K, Tomizawa Y, Sunaga N, Kawashima O, Oriuchi N, *et al*. ASC amino-acid transporter 2 (ASCT2) as a novel prognostic marker in non-small cell lung cancer. British Journal of Cancer. 2014; 110: 2030–2039.

[30] Nachef M, Ali AK, Almutairi SM, Lee SH. Targeting SLC1A5 and SLC3A2/SLC7A5 as a Potential Strategy to Strengthen Anti-Tumor Immunity in the Tumor Microenvironment. Frontiers in Immunology. 2021; 12: 624324.

[31] Tsai SJ, Hwang JM, Hsieh SC, Ying TH, Hsieh YH. Overexpression of myeloid zinc finger 1 suppresses matrix metalloproteinase-2 expression and reduces invasiveness of SiHa human cervical cancer cells. Biochemical and Biophysical Research Communications. 2012; 425: 462–467.

[32] Lin S, Wang X, Pan Y, Tian R, Lin B, Jiang G, *et al*. Transcription Factor Myeloid Zinc-Finger 1 Suppresses Human Gastric Carcinogenesis by Interacting with Metallothionein 2A. Clinical Cancer Research: an Official Journal of the American Association for Cancer Research. 2019; 25: 1050–1062.

[33] Martínez-Reyes I, Chandel NS. Cancer metabolism: looking forward. Nature Reviews. Cancer. 2021; 21: 669–680.

[34] Wu J, Song J, Yin X, Tang J, Zhang J, Wang X, *et al*. Recent Advancements of Nanotechnology-Based Strategies for Overcoming Tumor Microenvironment Hypoxia. Frontiers in Bioscience-Landmark. 2022; 27: 145.

[35] Kato Y, Maeda T, Suzuki A, Baba Y. Cancer metabolism: New insights into classic characteristics. The Japanese Dental Science Review. 2018; 54: 8–21.

[36] Mossmann D, Park S, Hall MN. mTOR signalling and cellular metabolism are mutual determinants in cancer. Nature Reviews. Cancer. 2018; 18: 744–757.

[37] Choi BH, Coloff JL. The Diverse Functions of Non-Essential Amino Acids in Cancer. Cancers. 2019; 11: 675.

[38] Wise DR, Thompson CB. Glutamine addiction: a new therapeutic target in cancer. Trends in Biochemical Sciences. 2010; 35: 427–433.

[39] Andergassen D, Rinn JL. From genotype to phenotype: genetics of mammalian long non-coding RNAs *in vivo*. Nature Reviews. Genetics. 2022; 23: 229–243.

[40] Deng SJ, Chen HY, Zeng Z, Deng S, Zhu S, Ye Z, *et al*. Nutrient Stress-Dysregulated Antisense lncRNA GLS-AS Impairs GLS-Mediated Metabolism and Represses Pancreatic Cancer Progression. Cancer Research. 2019; 79: 1398–1412.

[41] Wei L, Sun J, Zhang N, Zheng Y, Wang X, Lv L, *et al*. Noncoding RNAs in gastric cancer: implications for drug resistance. Molecular Cancer. 2020; 19: 62.

[42] Duan J, Huang Z, Nice EC, Xie N, Chen M, Huang C. Current advancements and future perspectives of long noncoding RNAs in lipid metabolism and signaling. Journal of Advanced Research. 2023; 48: 105–123.

[43] Kandasamy P, Gyimesi G, Kanai Y, Hediger MA. Amino acid transporters revisited: New views in health and disease. Trends in Biochemical Sciences. 2018; 43: 752–789.

[44] Canul-Tec JC, Assal R, Cirri E, Legrand P, Brier S, Chamot-Rooke J, *et al*. Structure and allosteric inhibition of excitatory amino acid transporter 1. Nature. 2017; 544: 446–451.

[45] Zhuang X, Tong H, Ding Y, Wu L, Cai J, Si Y, *et al*. Long noncoding RNA ABHD11-AS1 functions as a competing endogenous RNA to regulate papillary thyroid cancer progression by miR-199a-5p/SLC1A5 axis. Cell Death & Disease. 2019; 10: 620.

[46] Bhutia YD, Babu E, Ramachandran S, Ganapathy V. Amino Acid transporters in cancer and their relevance to "glutamine addiction": novel targets for the design of a new class of anticancer drugs. Cancer Research. 2015; 75: 1782–1788.

[47] Li Y, Li B, Xu Y, Qian L, Xu T, Meng G, *et al*. GOT2 Silencing Promotes Reprogramming of Glutamine Metabolism and Sensitizes Hepatocellular Carcinoma to Glutaminase Inhibitors. Cancer Research. 2022; 82: 3223–3235.

[48] Liu D, Lin J, Su J, Chen X, Jiang P, Huang K. Glutamine Deficiency Promotes PCV2 Infection through Induction of Autophagy via Activation of ROS-Mediated JAK2/STAT3 Signaling Pathway. Journal of Agricultural and Food Chemistry. 2018; 66: 11757–11766.

[49] Ma X, Cai D, Zhu Y, Zhao Y, Shang X, Wang C, *et al*. L-Glutamine alleviates osteoarthritis by regulating lncRNA-NKILA expression through the TGF-$\beta$1/SMAD2/3 signalling pathway. Clinical Science (London, England: 1979). 2022; 136: 1053–1069.

[50] Feng Y, Pathria G, Heynen-Genel S, Jackson M, James B, Yin J, *et al*. Identification and Characterization of IMD-0354 as a Glutamine Carrier Protein Inhibitor in Melanoma. Molecular Cancer Therapeutics. 2021; 20: 816–832.

[51] Jin H, Wang S, Zaal EA, Wang C, Wu H, Bosma A, *et al*. A powerful drug combination strategy targeting glutamine addiction for the treatment of human liver cancer. eLife. 2020; 9: e56749.

[52] Peterson FC, Hayes PL, Waltner JK, Heisner AK, Jensen DR, Sander TL, *et al*. Structure of the SCAN domain from the tumor suppressor protein MZF1. Journal of Molecular Biology. 2006; 363: 137–147.

[53] Brix DM, Bundgaard Clemmensen KK, Kallunki T. Zinc Finger Transcription Factor MZF1-A Specific Regulator of Cancer Invasion. Cells. 2020; 9: 223.

[54] Kanojia D, Panek WK, Cordero A, Fares J, Xiao A, Savchuk S, *et al*. BET inhibition increases $\beta$III-tubulin expression and sensitizes metastatic breast cancer in the brain to vinorelbine. Science Translational Medicine. 2020; 12: eaax2879.

[55] Vishwamitra D, Curry CV, Alkan S, Song YH, Gallick GE, Kaseb AO, *et al*. The transcription factors Ik-1 and MZF1 downregulate IGF-IR expression in NPM-ALK$^+$ T-cell lymphoma. Molecular Cancer. 2015; 14: 53.